Journal of Computational Physics 295 (2015) 685–714

Contents lists available at ScienceDirect

Journal of Computational Physics

www.elsevier.com/locate/jcp

A local discontinuous Galerkin method for the (non)-isothermal Navier–Stokes–Korteweg equations

Lulu Tian [a], Yan Xu [b,*], J.G.M. Kuerten [a,c], J.J.W. van der Vegt [a]

[a] Mathematics of Computational Science Group, Dept. of Applied Mathematics, University of Twente, P.O. Box 217, 7500 AE, Enschede, The Netherlands
[b] School of Mathematical Sciences, University of Science and Technology of China, Hefei, Anhui 230026, PR China
[c] Computational Multiphase Flow, Dept. of Mechanical Engineering, Eindhoven University of Technology, P.O. Box 513, 5600 MB, Eindhoven, The Netherlands

ARTICLE INFO

Article history:
Received 10 September 2014
Received in revised form 31 March 2015
Accepted 16 April 2015
Available online 28 April 2015

Keywords:
Local discontinuous Galerkin method
(Non-)isothermal Navier–Stokes–Korteweg equations
Phase transition
Van der Waals equation of state
Implicit time integration
Accuracy and stability

ABSTRACT

In this article, we develop a local discontinuous Galerkin (LDG) discretization of the (non)-isothermal Navier–Stokes–Korteweg (NSK) equations in conservative form. These equations are used to model the dynamics of a compressible fluid exhibiting liquid–vapor phase transitions. The NSK-equations are closed with a Van der Waals equation of state and contain third order nonlinear derivative terms. These contributions frequently cause standard numerical methods to violate the energy dissipation relation and require additional stabilization terms to prevent numerical instabilities. In order to address these problems we first develop an LDG method for the isothermal NSK equations using discontinuous finite element spaces combined with a time-implicit Runge–Kutta integration method. Next, we extend the LDG discretization to the non-isothermal NSK equations. An important feature of the LDG discretizations presented in this article is that they are relatively simple, robust and do not require special regularization terms. Finally, computational experiments are provided to demonstrate the capabilities, accuracy and stability of the LDG discretizations.

1. Introduction

In this article, we will present a local discontinuous Galerkin (LDG) method for the numerical solution of the Navier–Stokes–Korteweg (NSK) equations that model liquid–vapor phase transitions. This research is motivated by our previous work [35], where we solved a mixed hyperbolic–elliptic system that models phase transitions in solids and fluids using an LDG method. In that article, L_2-stability of the LDG discretization of the phase transition model was proved, and an error estimate for the LDG discretization for the viscosity–capillarity (VC) system with linear strain-stress relation was provided. The numerical experiments discussed in [35] show that the LDG method for the VC system is stable and the LDG solutions converge to the analytical solution of the original problem.

Two-phase flows can be treated either by sharp interface models or by diffuse interface models. Sharp interface models assume that the interface thickness is equal to zero and have successfully been applied to many two-phase flows

* Corresponding author.
E-mail addresses: l.tian@utwente.nl (L. Tian), yxu@ustc.edu.cn (Y. Xu), J.G.M.Kuerten@tue.nl (J.G.M. Kuerten), j.j.w.vandervegt@utwente.nl (J.J.W. van der Vegt).

http://dx.doi.org/10.1016/j.jcp.2015.04.025
0021-9991/

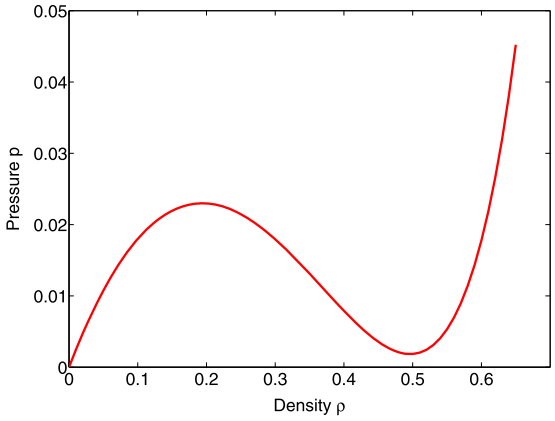

Fig. 1. Van der Waals type of pressure–density relation at the dimensionless temperature $\theta = 0.85$, gas constant $R = \frac{8}{27}$, and coefficients $a = 1.0$, $b = 1.0$.

[4,11,10,36]. Sharp interface models require, however, an extra evolution equation for the interface and face challenges in the reconstruction of the interface, leading to mathematical models that are solved by a Level Set or a Volume of Fluid method [23]. In contrast, diffuse interface models [3,6,40,33] regard the interface as thin layers of fluid where properties such as mass density, viscosity and pressure change smoothly. In the diffuse interface model, only a single set of governing equations needs to be solved on the entire flow domain, including the interface area. The Navier–Stokes–Korteweg (NSK) equations [17,31,32,5,29] contain an additional contribution to the stress tensor related to capillary forces and are an example of a diffuse interface model. The NSK equations are used in this article to model the dynamics of a compressible fluid exhibiting phase transitions between liquid and vapor.

We consider a fluid in a domain $\Omega \in \mathbb{R}^d$ with $d \leq 3$, and let ρ be the density of the fluid and $\mathbf{u}$ the velocity. The isothermal NSK equations with zero external forces, in dimensionless and conservative form, read

$$\begin{aligned} &\frac{\partial \rho}{\partial t} + \nabla \cdot (\rho \mathbf{u}) = 0, \\ &\frac{\partial (\rho \mathbf{u})}{\partial t} + \nabla \cdot (\rho \mathbf{u} \otimes \mathbf{u} + p\mathbf{I}) - \nabla \cdot \tau - \nabla \cdot \boldsymbol{\xi} = \mathbf{0}, \end{aligned} \tag{1}$$

in $\Omega \times (0, T]$, with p the pressure, $\otimes$ the tensor product and $\mathbf{I}$ the identity matrix. The viscous stress tensor $\boldsymbol{\tau}$ and Korteweg stress tensor $\boldsymbol{\xi}$ are given by

$$\begin{aligned} \boldsymbol{\tau} &= \frac{1}{\mathbb{R}e} \left(\nabla \mathbf{u} + \nabla^T \mathbf{u} - \frac{2}{3} \nabla \cdot \mathbf{u} \mathbf{I} \right), \\ \boldsymbol{\xi} &= \frac{1}{\mathbb{W}e} \left(\left(\rho \triangle \rho + \frac{1}{2} |\nabla \rho|^2 \right) \mathbf{I} - \nabla \rho \nabla^T \rho \right), \end{aligned} \tag{2}$$

where $\mathbb{R}e$, $\mathbb{W}e$ are the Reynolds number and Weber number. The definition of the dimensionless variables is summarized in Appendix A. To simulate phase transitions between liquid and vapor, which are distinguished by different values of the density ρ, we need an expression for the thermodynamic pressure that is valid in both liquid and vapor state. The Van der Waals equation of state is an appropriate choice, especially close to the critical temperature. For the isothermal NSK equations, we use the following dimensionless form [29,16]

$$p(\theta, \rho) = \frac{8}{27} \frac{\theta \rho}{(1 - \rho)} - \rho^2, \tag{3}$$

with θ the dimensionless temperature. Fig. 1 describes the shape of the Van der Waals type equation of state (3) for temperature $\theta = 0.85$.

Other relevant thermodynamic quantities for (non)-isothermal fluids [29,14] are the free energy density

$$W(\rho, \theta) = R\theta \rho \log \left(\frac{\rho}{b - \rho} \right) - a\rho^2,$$

and the chemical potential

$$\mu(\rho, \theta) = R\theta \log \left(\frac{\rho}{b - \rho} \right) + R\theta \frac{b}{b - \rho} - 2a\rho.$$

For isothermal flows, the total energy can be defined as

$$\mathcal{E}(\rho, \rho\mathbf{u}) = \int_{\Omega} \left(W(\rho) + \frac{1}{2\mathbb{W}e} |\nabla\rho|^2 + \frac{1}{2} \frac{|\rho\mathbf{u}|^2}{\rho} \right) d\mathbf{x}, \tag{4}$$

and satisfies for periodic boundary conditions the relation [29,16,5,33]

$$\frac{d}{dt}\mathcal{E}(\rho(\cdot,t), \rho\mathbf{u}(\cdot,t)) = -\int_{\Omega} \nabla\mathbf{u} : \boldsymbol{\tau} d\mathbf{x} \leq 0, \tag{5}$$

for positive $\mathbb{R}e$. Here ":" is summation of the element-wise product of two matrices. Suppose $A = (a_{ij})$, $B = (b_{ij}) \in \mathbb{R}^{d\times d}$, then $A : B = \sum_i \sum_j a_{ij} b_{ij}$.

An important question is the solvability of the isothermal NSK equations, which has received considerable attention. For isothermal NSK equations, local and global smooth solutions for Cauchy problems of (1) with constant coefficients and small, smooth initial data were discussed in [21,22]; the extension to Lipschitz continuous viscous coefficients and more general initial conditions was presented in [26]. In [33] a mathematical model with physically relevant non-local energies was proposed instead of the Van der Waals free energy and a short-time existence theorem for the Cauchy problem of the non-local NSK equations was proved. The existence of strong solutions and global weak solutions of the isothermal NSK system (1) modeling compressible fluids of Korteweg type was discussed in [12,20].

As discussed in [1,35], it is not trivial to obtain a numerical solution of mixed hyperbolic–elliptic systems. When it comes to the more complex mixed system (1), the non-monotonic Van der Waals equation of state can induce instabilities in the numerical solution. And the third order spatial derivatives of the mass density, stemming from the divergence of the Korteweg tensor $\boldsymbol{\xi}$, causes dispersive behavior of the numerical solution. Therefore numerical methods for the isothermal NSK equations face several challenges. One difficulty is that standard numerical methods including finite difference, finite volume, and discontinuous Galerkin (DG) methods with poor numerical fluxes, may violate the energy dissipation relation (5) and suffer from an increase in energy for multiphase flows [14]. Another problem is the occurrence of parasitic currents: unphysical velocities close to the interface. In particular, the velocity field does not tend to zero when equilibrium is approached [14,16]. In [24], a method is presented to eliminate parasitic currents for finite volume methods, but this is still a topic of ongoing research. Moreover, to capture the interface accurately requires locally a fine mesh.

Many articles addressed the numerical solution of the isothermal Navier–Stokes–Korteweg equations modeling liquid–vapor flows with phase change. A detailed description of higher order schemes, including the local discontinuous Galerkin method, to solve the non-conservative form of the isothermal NSK equations was given in [14]. A finite element formulation based on an isogeometric analysis of the non-conservative form of the isothermal NSK equations was developed in [17]. This method can straightforwardly deal with the higher-order derivatives in the isothermal NSK equations. In [29] a semi-discrete Galerkin method based on entropy variables and a new time integration scheme was proposed for the non-conservative form of the isothermal NSK equations. A DG scheme for the non-conservative form of the isothermal NSK equations, obtained by choosing special numerical fluxes, was presented in [16]. Another way to obtain a stable numerical discretization of the isothermal NSK equations is by adding two vanishing regularization terms. This approach was successfully used in [5] in combination with globally continuous finite element spaces and a time-implicit discretization.

The non-isothermal NSK equations [3,32] model two-phase flows involving phase transition at nonuniform temperatures. Besides the isothermal equations (1), the non-isothermal NSK equations also contain an equation for the total energy

$$\begin{aligned}
&\frac{\partial\rho}{\partial t} + \nabla\cdot(\rho\mathbf{u}) = 0, \\
&\frac{\partial\rho\mathbf{u}}{\partial t} + \nabla\cdot(\rho\mathbf{u}\otimes\mathbf{u} + p\mathbf{I}) - \nabla\cdot\tau - \nabla\cdot\boldsymbol{\xi} = \mathbf{0}, \\
&\frac{\partial(\rho E)}{\partial t} + \nabla\cdot((\rho E + p)\mathbf{u}) - \nabla\cdot((\boldsymbol{\tau} + \boldsymbol{\xi})\cdot\mathbf{u}) + \nabla\cdot\mathbf{q} + \nabla\cdot\mathbf{j}_E = 0,
\end{aligned} \tag{6}$$

where the total energy density is given by

$$\rho E = \rho e + \frac{1}{2}\rho|\mathbf{u}|^2 + \frac{1}{2}\frac{1}{\mathbb{W}e}|\nabla\rho|^2. \tag{7}$$

For the non-isothermal NSK equations (6), the dimensionless Van der Waals equation of state is given by [32,13]

$$p = \frac{8\theta\rho}{3-\rho} - 3\rho^2. \tag{8}$$

The specific internal energy e in (7) is given by

$$e = \frac{8}{3}C_v\theta - 3\rho,$$

with C_v the specific heat at constant volume. The total entropy is specified as $S = \rho s$ with s the entropy density

$$s = -\frac{8}{3}\log\left(\frac{\rho}{3-\rho}\right) + \frac{8}{3}C_v\log(\theta).$$

The heat flux $\mathbf{q}$ and energy flux $\mathbf{j}_E$ through the interface in (6) are defined as

$$\mathbf{q} = -\frac{8C_v}{3\mathbb{W}e\mathbb{P}r}\nabla\theta, \quad \mathbf{j}_E = \frac{1}{\mathbb{W}e}(\rho\nabla\cdot\mathbf{u})\nabla\rho, \tag{9}$$

where $\mathbb{P}r$ is the Prandtl number, see Appendix A. Recently global existence and uniqueness of strong solutions to the non-isothermal NSK equations were proved for bounded domains in [27,28].

Most articles so far only discuss the non-conservative form of the isothermal NSK equations (1). Frequently, the isothermal NSK equations (1) are rewritten into an extended system by adding an extra variable for the total energy equation [29,16,5,33]. It is, however, not trivial to do this for the non-isothermal NSK equations, where the Van der Waals equation of state depends on both the density and temperature, so the frequently used relation

$$\nabla p = \rho\nabla W'(\rho)$$

is no longer satisfied. The numerical methods for the isothermal NSK equations discussed in [29,16,5,33] are therefore difficult to extend to the non-isothermal NSK equations. The great potential of the LDG method to solve phase transition problems, as shown in [18,35], motivated us to develop an LDG method for systems (1) and (6), while keeping the conservative form of the (non)-isothermal NSK equations and obtain a stable numerical discretization without additional regularization terms. To our knowledge, we are the first to discuss an LDG method for the conservative form of the (non)-isothermal NSK equations.

The LDG method is an extension of the discontinuous Galerkin (DG) method that aims to solve partial differential equations (PDEs) containing higher order spatial derivatives and was originally developed by Cockburn and Shu in [9] for solving nonlinear convection–diffusion equations containing second-order spatial derivatives. The idea behind LDG methods is to rewrite the original equations as a first order system, and then apply the DG method to this first order system. The design of the numerical fluxes is the key ingredient to ensure stability. LDG techniques have been developed for convection–diffusion equations [9], nonlinear KdV type equations [39], the Camassa–Holm equation [37] and many other types of partial differential equations. For a review, see [38]. The LDG method results in an extremely local discretization, which offers great advantages in parallel computing and *hp*-adaptation.

The organization of this article is as follows. In Section 2 we present the LDG method for the (non)-isothermal NSK equations in detail. An important aspect of this discretization is that it preserves the conservative form of the NSK equations. Section 3 discusses an implicit Runge–Kutta time integration method, which is used to overcome the stiffness of the NSK equations. In Section 4, numerical experiments are presented to investigate the accuracy and stability of the LDG discretization of the (non)-isothermal NSK equations. For the isothermal NSK equations, discrete mass conservation and energy dissipation are verified for the LDG solutions, while the mass conservation and total entropy are verified for the non-isothermal NSK equations. Finally, we give conclusions in Section 5.

2. LDG discretization of the NSK system

In this section, we develop an LDG method to solve the (non)-isothermal NSK system in $\Omega \in \mathbb{R}^d$ with $d \leq 3$. We restrict the numerical experiments to one and two dimensions in this paper, but the LDG discretization described here can be easily extended to three dimensions. We first introduce notations used for the description of the LDG discretization.

2.1. Notations

We denote by $\mathcal{T}_h$ a tessellation of Ω with regular shaped elements K, Γ represents all boundary faces of $K \in \mathcal{T}_h$ and $\Gamma_0 = \Gamma\backslash\partial\Omega$. Suppose e is a face shared by the "left" and "right" elements K_L and K_R. The normal vectors $\mathbf{n}_L$ and $\mathbf{n}_R$ on e point, respectively, exterior to K_L and K_R. Let φ be a function on K_L and K_R, which could be discontinuous across e, then the left and right trace are denoted as $\varphi_L = (\varphi|_{K_L})|_e$, $\varphi_R = (\varphi|_{K_R})|_e$, respectively. For more details about these definitions, we refer the reader to [38].

For the LDG discretization, we define the finite element spaces

$$V_h = \{\phi \in L^2(\Omega) : \phi|_K \in \mathcal{P}^k(K), \forall K \in \mathcal{T}_h\},$$
$$\Sigma_h^d = \{\mathbf{\Phi} = (\phi^{(1)}, \phi^{(2)}, \ldots, \phi^{(d)})^T \in (L^2(\Omega))^d : \phi^{(i)}|_K \in \mathcal{P}^k(K), \quad i = 1, \ldots, d, \forall K \in \mathcal{T}_h\},$$

with $\mathcal{P}^k(K)$ the space of polynomials of degree up to $k \geq 0$ on $K \in \mathcal{T}_h$.

The numerical solution is denoted by $\mathbf{U}_h$, with each component of $\mathbf{U}_h$ belonging to the finite element space V_h, and can be written as

$$\mathbf{U}_h(\mathbf{x}, t)|_K = \sum_{l=0}^{N_p} \widehat{\mathbf{U}}_l^K(t)\phi_l(\mathbf{x}), \text{ for } \mathbf{x} \in K. \tag{10}$$

Here, $\widehat{\mathbf{U}}_l^K(t)$ are unknowns and Legendre polynomials are used for the basis functions $\phi_l(\mathbf{x})$. In the next two sections we will discuss a local discontinuous Galerkin discretization for both the isothermal and non-isothermal NSK equations. We first consider the isothermal NSK equations since they provide a simpler model for phase transitions and are frequently used in applications. The non-isothermal NSK equations are computationally more demanding, but provide a more realistic model of the complex physics of phase transition.

2.2. LDG discretization for the isothermal NSK equations

In this section, we propose an LDG discretization for the isothermal NSK equations, which are rewritten as a first order system, given by the primary equations

$$\begin{aligned}
&\rho_t + \nabla\cdot\mathbf{m} = 0,\\
&\mathbf{m}_t + \nabla\cdot\mathbf{F}(\mathbf{U}) - \nabla\cdot\tau(\mathbf{z}, l) - \nabla\cdot\boldsymbol{\xi}(\rho, \mathbf{r}, g) = \mathbf{0},
\end{aligned} \tag{11}$$

and auxiliary equations

$$\begin{aligned}
&\mathbf{z} = \nabla\mathbf{u},\\
&l = \nabla\cdot\mathbf{u},\\
&\mathbf{r} = \nabla\rho,\\
&g = \nabla\cdot\mathbf{r},
\end{aligned} \tag{12}$$

where

$$\begin{aligned}
&\mathbf{u} = \frac{\mathbf{m}}{\rho},\\
&\boldsymbol{\tau} = \frac{1}{\mathbb{R}e}\left(\mathbf{z} + \mathbf{z}^T - \frac{2}{3}l\mathbf{I}\right),\\
&\boldsymbol{\xi} = \frac{1}{\mathbb{W}e}\left(\left(\rho g + \frac{1}{2}|\mathbf{r}|^2\right)\mathbf{I} - \mathbf{r}\mathbf{r}^T\right),
\end{aligned} \tag{13}$$

and

$$\mathbf{F}(\mathbf{U}) = \mathbf{m}\otimes\mathbf{u} + p(\rho)\mathbf{I}, \quad \mathbf{U} = \begin{pmatrix}\rho\\ \mathbf{m}\end{pmatrix}.$$

The LDG discretization for the isothermal NSK equations (11)–(13) is now as follows: find $\rho_h, l_h, g_h \in V_h$, and $\mathbf{m}_h, \mathbf{z}_h, \mathbf{r}_h \in \Sigma_h^d$, such that for all test functions $\phi, \varphi, \zeta \in V_h$ and $\psi, \eta, \varsigma \in \Sigma_h^d$, the following relations are satisfied

$$\begin{aligned}
&\int_K (\rho_h)_t\phi\, dK - \int_K \mathbf{m}_h\cdot\nabla\phi\, dK + \int_{\partial K}\widehat{\mathbf{m}_h}\cdot\mathbf{n}\phi\, ds = 0,\\
&\int_K (\mathbf{m}_h)_t\psi\, dK - \int_K (\mathbf{F}_h - \boldsymbol{\tau}_h - \boldsymbol{\xi}_h)\cdot\nabla\psi\, dK + \int_{\partial K}(\widehat{\mathbf{F}_h} - \widehat{\boldsymbol{\tau}_h} - \widehat{\boldsymbol{\xi}_h})\cdot\mathbf{n}\psi\, ds = \mathbf{0},
\end{aligned} \tag{14}$$

and

$$\begin{aligned}
&\int_K \mathbf{z}_h\eta\, dK = -\int_K \mathbf{u}_h\nabla\cdot\eta\, dK + \int_{\partial K}\widehat{\mathbf{u}_h}\eta\cdot\mathbf{n}\, ds,\\
&\int_K l_h\zeta\, dK = -\int_K \mathbf{u}_h\cdot\nabla\zeta\, dK + \int_{\partial K}\widehat{\mathbf{u}_h}\cdot\mathbf{n}\zeta\, ds,\\
&\int \mathbf{r}_h\varsigma\, dK = -\int_K \rho_h\nabla\cdot\varsigma\, dK + \int_{\partial K}\widehat{\rho_h}\varsigma\cdot\mathbf{n}\, ds,\\
&\int_K g_h\varphi\, dK = -\int_K \mathbf{r}_h\cdot\nabla\varphi\, dK + \int_{\partial K}\widehat{\mathbf{r}_h}\cdot\mathbf{n}\varphi\, ds,
\end{aligned} \tag{15}$$

where

$$\widehat{\mathbf{u}}_h = \frac{\widehat{\mathbf{m}}_h}{\widehat{\rho}_h},$$
$$\widehat{\boldsymbol{\tau}}_h = \frac{1}{\mathbb{R}e}\left(\widehat{\mathbf{z}}_h + \widehat{\mathbf{z}}_h^T - \frac{2}{3}\widehat{l}_h\mathbf{I}\right),$$
$$\widehat{\boldsymbol{\xi}}_h = \frac{1}{\mathbb{W}e}\left(\left(\widehat{\rho}_h\widehat{g}_h + \frac{1}{2}|\widehat{\mathbf{r}}_h|^2\right)I - \widehat{\mathbf{r}}_h\widehat{\mathbf{r}}_h^T\right), \tag{16}$$

and

$$\mathbf{F}_h = \mathbf{F}(\mathbf{U}_h), \quad \mathbf{U}_h = \begin{pmatrix}\rho_h \\ \mathbf{m}_h\end{pmatrix}.$$

For the numerical fluxes in (14), (15) and (16), denoted with a hat, we choose the Lax–Friedrich flux for the convective part and central numerical fluxes for the other terms,

$$\widehat{\mathcal{F}_h}|_e = \frac{1}{2}(\mathcal{F}_h|_L + \mathcal{F}_h|_R - \alpha(\mathbf{U}_h|_R - \mathbf{U}_h|_L)), \quad \text{with } \mathcal{F}_h = \begin{pmatrix}\mathbf{m}_h \\ \mathbf{F}_h\end{pmatrix},$$
$$\widehat{\mathbf{m}}_h|_e = \frac{1}{2}(\mathbf{m}_h|_L + \mathbf{m}_h|_R), \quad \widehat{\rho}_h|_e = \frac{1}{2}(\rho_h|_L + \rho_h|_R),$$
$$\widehat{\mathbf{r}}_h|_e = \frac{1}{2}(\mathbf{r}_h|_L + \mathbf{r}_h|_R), \quad \widehat{\mathbf{z}}_h|_e = \frac{1}{2}(\mathbf{z}_h|_L + \mathbf{z}_h|_R),$$
$$\widehat{l}_h|_e = \frac{1}{2}(l_h|_L + l_h|_R), \quad \widehat{g}_h|_e = \frac{1}{2}(g_h|_L + g_h|_R), \tag{17}$$

with α a positive constant that is chosen as the maximum absolute eigenvalue of $\frac{\partial \mathcal{F}_h}{\partial \mathbf{U}_h}$ globally.

2.3. LDG discretization for the non-isothermal NSK equations

The LDG discretization for the isothermal NSK equations presented in Section 2.2 can be extended to the non-isothermal NSK equations (6). The equations can also be rewritten as a first order system that includes Eqs. (11)–(13) and additional equations given by

$$(\rho E)_t + \nabla\cdot\mathbf{G}(\mathbf{U}) - \nabla\cdot((\tau+\boldsymbol{\xi})\cdot\mathbf{u}) + \nabla\cdot\mathbf{q} + \nabla\cdot\mathbf{j}_E = 0, \tag{18}$$
$$\mathbf{q} = -\frac{8C_v}{3\mathbb{W}e\mathbb{P}r}\nabla\theta, \tag{19}$$
$$\mathbf{j}_E = \frac{1}{\mathbb{W}e}\rho l\mathbf{r}, \quad \mathbf{G}(\mathbf{U}) = (\rho E + p)\mathbf{u}.$$

The LDG discretization for the non-isothermal NSK equations contains (14)–(16), and the LDG discretization for the energy equation contributions, given by (18), can be written as

$$\int_K ((\rho E)_h)_t\chi\, dK - \int_K (\mathbf{G}_h - (\boldsymbol{\tau}_h + \boldsymbol{\xi}_h)\cdot\mathbf{u}_h + \mathbf{q}_h + (\mathbf{j}_E)_h)\cdot\nabla\chi\, dK$$
$$+ \int_{\partial K}(\widehat{\mathbf{G}_h} - (\widehat{\tau_h} + \widehat{\xi_h})\cdot\widehat{\mathbf{u}_h} + \widehat{\mathbf{q}_h} + \widehat{(\mathbf{j}_E)_h})\cdot\mathbf{n}\chi\, ds = 0. \tag{20a}$$
$$\int_K \mathbf{q}_h\boldsymbol{\sigma}\, dK - \frac{8C_v}{3\mathbb{W}e\mathbb{P}r}\int_K \theta_h\nabla\cdot\boldsymbol{\sigma}\, dK + \frac{8C_v}{3\mathbb{W}e\mathbb{P}r}\int_{\partial K}\widehat{\theta_h}\boldsymbol{\sigma}\cdot\mathbf{n}\, ds = 0, \tag{20b}$$

with

$$(\mathbf{j}_E)_h = \frac{1}{\mathbb{W}e}\rho_h l_h\mathbf{r}_h,\ \mathbf{G}_h = \mathbf{G}(\mathbf{U}_h) \text{ and } \mathbf{U}_h = \begin{pmatrix}\rho_h \\ \mathbf{m}_h \\ (\rho E)_h\end{pmatrix}.$$

The same numerical fluxes (17) as used in the LDG discretization for the isothermal NSK equations are used in the non-isothermal equations. If we denote $\mathcal{G}_h(\mathbf{U}_h) = \begin{pmatrix}\mathcal{F}_h \\ \mathbf{G}_h\end{pmatrix}$, then the numerical flux for $\mathcal{G}_h$ is also the Lax–Friedrichs flux, but now with the constant α the maximum absolute eigenvalue of $\frac{\partial \mathcal{G}_h}{\partial \mathbf{U}_h}$. For the one-dimensional case the eigenvalues of $\frac{\partial \mathcal{G}_h}{\partial \mathbf{U}_h}$ are

provided in [13]. For two-dimensional case, u, v are additional eigenvalues in, respectively x and y direction. The additional numerical fluxes in the energy equation contributions (20) are chosen as

$$\widehat{\mathbf{q}_h} = \frac{1}{2}(\mathbf{q}_h|_L + \mathbf{q}_h|_R), \quad \widehat{\theta_h} = \frac{1}{2}(\theta_h|_L + \theta_h|_R), \quad \widehat{(\mathbf{j}_E)_h} = \frac{1}{\mathbb{W}e}\widehat{\rho_h}\widehat{l_h}\widehat{\mathbf{r}_h}. \tag{21}$$

Remark 2.1. We emphasize that not only the (first-order) convective part of the isothermal NSK equations (11), but also the (first-order) convective part of the non-isothermal NSK equations is of mixed hyperbolic–elliptic type. The eigenvalues of the systems are given explicitly below. The convective part of the isothermal NSK equations is given by

$$\begin{aligned} &\frac{\partial \rho}{\partial t} + \nabla \cdot (\rho \mathbf{u}) = 0, \\ &\frac{\partial (\rho \mathbf{u})}{\partial t} + \nabla \cdot (\rho \mathbf{u} \otimes \mathbf{u} + p) = 0. \end{aligned} \tag{22}$$

In 2D, assuming $\mathbf{u} = (u, v)^T$, the Jacobian matrices are

$$A^1 = \begin{pmatrix} 0 & 1 & 0 \\ -u^2 + p'(\rho) & 2u & 0 \\ -uv & v & u \end{pmatrix}, \quad A^2 = \begin{pmatrix} 0 & 0 & 1 \\ -uv & v & u \\ -v^2 + p'(\rho) & 0 & 2v \end{pmatrix}$$

for, respectively, the x- and y-direction. The eigenvalues of A^1 are $\{u - \sqrt{p'(\rho)},\ u,\ u + \sqrt{p'(\rho)}\}$ and those of A^2 are $\{v - \sqrt{p'(\rho)}, v, v + \sqrt{p'(\rho)}\}$. Consequently, (22) is a hyperbolic–elliptic system due to the non-monotonicity of the Van der Waals equation of state, and it is elliptic when $p'(\rho) < 0$.

The eigenvalues of the convective part of the one-dimensional non-isothermal NSK equations were studied in [13]. The eigenvalues of the 2D non-isothermal NSK equations are the extension of those of the 1D non-isothermal NSK equations, with one extra u, v, in the x, y direction respectively. In detail, the convective part of the non-isothermal NSK equations is rewritten, in primitive form, as

$$\mathbf{V}_t + \widetilde{F}(\mathbf{V})_x + \widetilde{G}(\mathbf{V})_y = 0, \quad \text{with } \mathbf{V} = (\rho,\ u,\ v,\ p) \text{ in 2D.}$$

The Jacobian matrices are given by

$$A^1 = \frac{\partial \widetilde{F}}{\partial \mathbf{V}} = \begin{pmatrix} u & \rho & 0 & 0 \\ 0 & u & 0 & 1/\rho \\ 0 & 0 & u & 0 \\ 0 & f(p,\rho) & 0 & u \end{pmatrix}, \quad A^2 = \frac{\partial \widetilde{G}}{\partial \mathbf{V}} = \begin{pmatrix} v & 0 & \rho & 0 \\ 0 & v & 0 & 0 \\ 0 & 0 & v & 1/\rho \\ 0 & 0 & f(p,\rho) & v \end{pmatrix},$$

where the function f is equal to

$$f(p,\rho) = \frac{3}{C_v(3-\rho)}\left((1 + C_v p + \rho^2(3 - 3C_v + 2C_v\rho))\right).$$

The eigenvalues of A^1 are $\{u,\ u,\ u - \sqrt{\beta},\ u + \sqrt{\beta}\}$, and those of A^2 are $\{v,\ v,\ v - \sqrt{\beta},\ v + \sqrt{\beta}\}$, with $\beta = 2\left(\frac{p}{\rho} + \frac{4\theta(3+C_v(-3+2\rho))}{C_v(-3+\rho)^2}\right)$.

3. Implicit time discretization method

The equations for the DG expansion coefficients for each variable are obtained by introducing the polynomial representation (10) into the LDG discretizations (14)–(16) and (20). The coefficients of the polynomial expansions of $\rho_h(\mathbf{x}, t)$, $\mathbf{m}_h(\mathbf{x}, t)$ and $\rho E_h(\mathbf{x}, t)$ in the LDG discretization are collected in the vector $\widehat{\mathbf{U}}(t)$. The LDG discretization, given by (14)–(16) and (20) with corresponding fluxes for $\rho_h(\mathbf{x}, t)$, $\mathbf{m}_h(\mathbf{x}, t)$ and $\rho E_h(\mathbf{x}, t)$, then results in a system of ordinary differential and algebraic equations (DAEs)

$$\begin{aligned} &\frac{d\widehat{\mathbf{U}}(t)}{dt} + \mathbf{L}(\widehat{\mathbf{U}}(t), \widehat{\mathbf{Z}}(t), \widehat{\mathbf{G}}(t)) = 0, \\ &\widehat{\mathbf{Z}}(t) - \mathbf{P}(\widehat{\mathbf{U}}(t)) = 0, \\ &\widehat{\mathbf{G}}(t) - \mathbf{Q}(\widehat{\mathbf{U}}(t), \widehat{\mathbf{Z}}(t)) = 0, \end{aligned} \tag{23}$$

with $\widehat{\mathbf{Z}}(t)$, $\widehat{\mathbf{G}}(t)$ the coefficients of the auxiliary variables, and $\mathbf{L}$, $\mathbf{P}$, $\mathbf{Q}$ nonlinear functions of $\widehat{\mathbf{U}}(t)$, $\widehat{\mathbf{Z}}(t)$, and $\widehat{\mathbf{G}}(t)$. The initial values are

$$\widehat{\mathbf{U}}(t_0) = \widehat{\mathbf{U}}_0.$$

Note, in case of the isothermal NSK equations, the contributions from (20) are missing. Both explicit and implicit time integration methods [19] can be applied to the DAE system (23). Due to the Korteweg stress tensor $\boldsymbol{\xi}$, the NSK system is a third order nonlinear system of partial differential equations, and explicit time integration methods then require the time step to satisfy

$$\Delta t = O(h^2), \quad h = \min\{\Delta x, \Delta y\}, \tag{24}$$

for stability [13]. Moreover, when we would consider local mesh refinement near the interface, the time step restriction (24) becomes even more severe. Therefore, we consider an implicit time stepping method.

3.1. Diagonally Implicit Runge–Kutta methods

For the implicit time integration we use Diagonally Implicit Runge–Kutta (DIRK) methods, since they allow that the equations for each implicit stage are solved in a sequential manner. A class of Diagonally Implicit Runge–Kutta (DIRK) formulae, which are A-stable and computationally efficient, was discussed in [2,8,19]. A special feature of the DIRK method in [8] is that it provides embedded DIRK formulae that allow a straightforward calculation of the local truncation error at each time step without extra computation. This provides an efficient way to estimate the time step required for a certain accuracy level. In [34] DIRK methods based on the minimization of certain error functions were considered, and several Butcher tables for specific DIRK formulae were given.

For the third order accurate LDG discretization in space, which uses quadratic basis functions, we use the third order Singly DIRK scheme from [34], given by

$$\begin{aligned}
&\widehat{\mathbf{U}}^{n1} = \widehat{\mathbf{U}}^{n} + \Delta t a_{11}\mathbf{K}_1, \quad \widehat{\mathbf{Z}}^{n1} = \mathbf{P}(\widehat{\mathbf{U}}^{n1}), \quad \mathbf{G}^{n1} = \mathbf{Q}(\widehat{\mathbf{U}}^{n1}, \widehat{\mathbf{Z}}^{n1}),\\
&\mathbf{K}_1 = -\mathbf{L}\left(t_n + c_1\Delta t, \widehat{\mathbf{U}}^{n1}, \widehat{\mathbf{Z}}^{n1}, \widehat{\mathbf{G}}^{n1}\right),\\
&\widehat{\mathbf{U}}^{n2} = \widehat{\mathbf{U}}^{n} + \Delta t a_{21}\mathbf{K}_1 + \Delta t a_{22}\mathbf{K}_2, \quad \widehat{\mathbf{Z}}^{n2} = \mathbf{P}(\widehat{\mathbf{U}}^{n2}), \quad \widehat{\mathbf{G}}^{n2} = \widehat{\mathbf{Q}}(\widehat{\mathbf{U}}^{n2}, \widehat{\mathbf{Z}}^{n2}),\\
&\mathbf{K}_2 = -\mathbf{L}\left(t_n + c_2\Delta t, \widehat{\mathbf{U}}^{n2}, \widehat{\mathbf{Z}}^{n2}, \widehat{\mathbf{G}}^{n2}\right),\\
&\widehat{\mathbf{U}}^{n3} = \widehat{\mathbf{U}}^{n} + \Delta t a_{31}\mathbf{K}_1 + \Delta t a_{32}\mathbf{K}_2 + \Delta t a_{33}\mathbf{K}_3, \quad \widehat{\mathbf{Z}}^{n3} = \mathbf{P}(\widehat{\mathbf{U}}^{n3}), \quad \widehat{\mathbf{G}}^{n3} = \mathbf{Q}(\widehat{\mathbf{U}}^{n3}, \widehat{\mathbf{Z}}^{n3}),\\
&\mathbf{K}_3 = -\mathbf{L}\left(t_n + c_3\Delta t, \widehat{\mathbf{U}}^{n3}, \widehat{\mathbf{Z}}^{n3}, \widehat{\mathbf{G}}^{n3}\right),\\
&\widehat{\mathbf{U}}^{n+1} = \widehat{\mathbf{U}}^{n} + \Delta t b_1\mathbf{K}_1 + \Delta t b_2\mathbf{K}_2 + \Delta t b_3\mathbf{K}_3.
\end{aligned}$$

The coefficients in the SDIRK scheme are defined in the Butcher table

$$\begin{array}{c|c|ccc}
\mathbf{c} & \mathbf{A} & & & \\
\hline
\frac{\gamma}{\frac{1+\gamma}{2}} & \frac{\gamma}{\frac{1-\gamma}{2}} & & & \\
1 & 1-b_2-\gamma & b_2 & \gamma & \\
\hline
 & \mathbf{b}^T & 1-b_2-\gamma & b_2 & \gamma
\end{array}$$

with $b_2 = \frac{1}{4}(5 - 20\gamma + 6\gamma^2)$ and $\gamma = 0.43586652$. For the second order accurate LDG discretization in space, which uses linear polynomial basis functions, we use the second order accurate implicit Runge–Kutta time integration scheme

$$\begin{aligned}
&\widehat{\mathbf{U}}^{n1} = \widehat{\mathbf{U}}^{n} + \Delta t\frac{1}{2}\mathbf{K}_1, \quad \widehat{\mathbf{Z}}^{n1} = \mathbf{P}(\widehat{\mathbf{U}}^{n1}), \quad \widehat{\mathbf{G}}^{n1} = \widehat{\mathbf{Q}}(\widehat{\mathbf{U}}^{n1}, \widehat{\mathbf{Z}}^{n1}),\\
&\mathbf{K}_1 = -\mathbf{L}\left(t_n + \frac{1}{2}\Delta t, \widehat{\mathbf{U}}^{n1}, \widehat{\mathbf{Z}}^{n1}, \widehat{\mathbf{G}}^{n1}\right),\\
&\widehat{\mathbf{U}}^{n+1} = \widehat{\mathbf{U}}^{n} + \frac{1}{2}\Delta t\mathbf{K}_1.
\end{aligned} \tag{25}$$

Note that the intermediate stages $\mathbf{K}_1$, $\mathbf{K}_2$ and $\mathbf{K}_3$ must be solved implicitly, i.e. three (or one) large-scale nonlinear problems need to be dealt with. In recent years, great progress has been made in solving large nonlinear algebraic systems using globalized inexact Newton methods [15,30]. The main difficulty with classical Newton methods is that a large-scale linear system needs to be solved at each iteration, which can be costly with a direct solver. A popular alternative is a class of Newton–Krylov methods, which solve the large-scale nonlinear system iteratively. For more details, we refer to [25]. In the next section we describe the use of these methods to solve the nonlinear stage equations in the SDIRK method.

3.2. Newton–Krylov methods

Newton–Krylov methods solve the nonlinear equations

$$F(x) = 0, \quad \text{with } F \in \mathbb{R}^N, \tag{26}$$

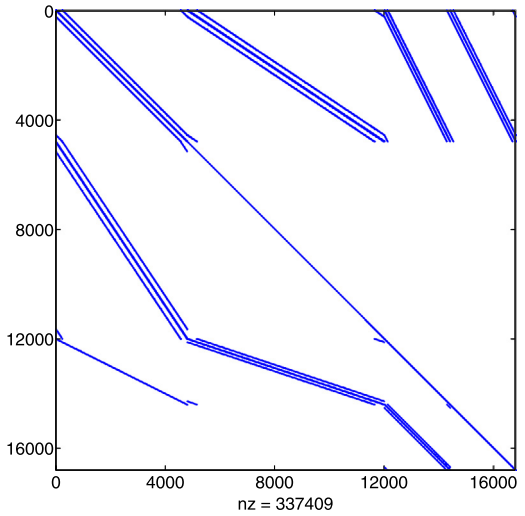

Fig. 2. Non-zeros in the Jacobian matrix for the LDG discretization of the two-dimensional non-isothermal NSK equations on a mesh with 20×20 elements.

in the following way: given an initial solution x_0, iteratively compute

$$x_{k+1} = x_k + s, \quad \text{with } s \text{ a solution of } DF(x_k)s = -F(x_k), \tag{27}$$

where x_k is the current approximate solution and $DF(x_k)$ the Jacobian matrix of $F(x)$ at x_k. These methods combine outer nonlinear Newton iterations with inner linear Krylov iterations. The inner iteration stops when

$$\|F(x_k) + DF(x_k)s_k\| \leq \eta_k \|F(x_k)\|, \tag{28}$$

where the constant $\eta_k \in (0, 1)$ can be either fixed or specified dynamically.

We take the second order implicit Runge–Kutta time integration method (25) to explain the computation of the Jacobian matrix. System (25) can be rewritten as

$$\begin{aligned}
&\mathbf{F}_1 \triangleq \mathbf{K}_1 + \mathbf{L}\left(t_n + \frac{1}{2}\Delta t, \widehat{\mathbf{U}}^{n1}, \widehat{\mathbf{Z}}^{n1}, \widehat{\mathbf{G}}^{n1}\right) = 0,\\
&\mathbf{F}_2 \triangleq \widehat{\mathbf{Z}}^{n1} - \mathbf{P}(\widehat{\mathbf{U}}^{n1}) = 0,\\
&\mathbf{F}_3 \triangleq \widehat{\mathbf{G}}^{n1} - \mathbf{Q}(\widehat{\mathbf{U}}^{n1}, \widehat{\mathbf{Z}}^{n1}) = 0
\end{aligned}$$

with $\widehat{\mathbf{U}}^{n1} = \widehat{\mathbf{U}}^{n} + \Delta t \frac{1}{2}\mathbf{K}_1$. The Jacobian matrix $\mathbf{J}$ has the structure

$$\mathbf{J} = \begin{pmatrix}
\frac{\partial \mathbf{F}_1}{\partial \mathbf{K}_1} & \frac{\partial \mathbf{F}_1}{\partial \widehat{\mathbf{Z}}^{n1}} & \frac{\partial \mathbf{F}_1}{\partial \widehat{\mathbf{G}}^{n1}} \\
\frac{\partial \mathbf{F}_2}{\partial \mathbf{K}_1} & \frac{\partial \mathbf{F}_2}{\partial \widehat{\mathbf{Z}}^{n1}} & \mathbf{0} \\
\frac{\partial \mathbf{F}_3}{\partial \mathbf{K}_1} & \frac{\partial \mathbf{F}_3}{\partial \widehat{\mathbf{Z}}^{n1}} & \frac{\partial \mathbf{F}_3}{\partial \widehat{\mathbf{G}}^{n1}}
\end{pmatrix}$$

which is shown in Fig. 2. It is not practical to solve the linear system in (27), with $DF(x_k)$ as Jacobian matrix, using a direct method. The linear system is therefore solved using GMRES with an ILU(0) preconditioner in order to prevent a large fill-in of the matrix.

4. Numerical experiments

In this section, we perform several numerical experiments to investigate the stability and accuracy of the LDG schemes for the (non)-isothermal NSK equations proposed in Sections 2.2 and 2.3. The examples in Section 4.2 are test cases for the isothermal NSK equations, including an investigation of the order of accuracy, a few one-dimensional benchmark problems and a two-dimensional simulation of the coalescence of two bubbles. These model problems were recently also (partly) studied in [29,5] using a semi-discrete Galerkin method and a continuous finite element method, together with special time integration schemes. Compared to these methods the LDG schemes that we present in this article are relatively simple, robust and do not require additional regularization terms. The simulations of the non-isothermal NSK equations (6) are presented in Section 4.3, including accuracy verification, a static Riemann problem and a two-dimensional simulation of bubble coalescence. Note that we did not use any limiter in the computations. Periodic boundary conditions and a uniform mesh are applied for all test cases.

We use implicit Runge–Kutta (RK) time integration methods to solve the ODE system resulting from the LDG discretization for the accuracy tests and two-dimensional bubble coalescence simulations. In the accuracy tests, the time step is chosen as $dt = 0.8h$ for the third order implicit RK time method, with h the length of an element. The time step $dt = 1.5h$ is chosen for the second order implicit RK time method for the two-dimensional bubble coalescence tests.

In several numerical examples, an equilibrium state with an interface between liquid and vapor is used to verify the capabilities of the proposed LDG scheme, described in Section 2.2. The velocity is denoted by u in 1D, while $\mathbf{u} = (u, v)^T$ in 2D. At a certain dimensionless temperature $\theta < 1$ in the Van der Waals equation of state, the densities in the equilibrium state ρ_v, ρ_l that satisfy the following relations for the pressure and chemical potential

$$\begin{aligned} p(\theta, \rho_v) &= p(\theta, \rho_l), \\ \mu(\theta, \rho_v) &= \mu(\theta, \rho_l), \end{aligned} \tag{29}$$

are called Maxwell states.

4.1. Interface width

To resolve the diffuse interface accurately, a sufficiently fine mesh is required in a simulation of a phase-field problem, otherwise the numerical solution will contain non-physical oscillations [29]. Suppose that the Helmholtz free energy is denoted by f, and that Δf is the difference in Helmholtz free energy between the phase mixture and the separate phases:

$$\Delta f = f - f_0.$$

Here $f_0(\rho) = f(\rho_v, \theta_0) + (\rho - \rho_v)\frac{f(\rho_l,\theta_0) - f(\rho_v,\theta_0)}{\rho_l - \rho_v}$ for the given temperature θ_0. The interface thickness [7] is then given by

$$d = 2\frac{L}{\sqrt{\mathbb{W}e}}\frac{\rho_l - \rho_v}{\sqrt{\Delta f_{max}}}, \tag{30}$$

with Δf_{max} the maximum value of Δf, L the reference length scale and ρ_l, ρ_v the critical densities at a given temperature. From the numerical tests, we found that at least 10 mesh nodes are required inside the interface to capture the interface accurately and guarantee the stability of the energy or entropy. This gives the relation $d = \alpha h$, $\alpha > 10$ with h the mesh size in the interface region.

4.2. Numerical tests for the isothermal NSK equations

Similar to [5,29], choosing the temperature as $\theta = 0.85$ and the Van der Waals equation of state (3), the critical vapor and liquid densities are equal to $\rho_v = 0.106576655$, $\rho_l = 0.602380109$.

4.2.1. Accuracy test

In this section, we will study the accuracy of the LDG discretization for the isothermal NSK equations. To investigate the accuracy of the one-dimensional LDG discretization, we select an exact smooth solution as

$$\begin{aligned} \rho &= 0.6 + 0.1\sin(5\pi t)\cos(2\pi x), \\ u &= \sin(3\pi t)\sin(2\pi x), \end{aligned} \tag{31}$$

which satisfies (1) with an additional source term $\mathbf{S}$. The source terms are added artificially and obtained by inserting the chosen exact smooth solution (31) into (11). The computational domain is $\Omega = (0, 1)$, and the coefficients in (1) are

$$\mathbb{R}e = 20, \quad \mathbb{W}e = 100. \tag{32}$$

The solutions are obtained using the LDG discretization with piecewise linear and quadratic polynomials, combined with the third order implicit Runge–Kutta time integration method with stopping parameter η_k in (28) chosen as $\eta_k = 10^{-9}$. Table 1 shows the accuracy of the LDG scheme for the one-dimensional isothermal NSK equations. From this table, we can see that the LDG discretizations have optimal order of accuracy for the different polynomial orders.

To investigate the accuracy of the LDG discretization for the two-dimensional isothermal NSK equations, we choose an exact smooth solution

$$\begin{aligned} \rho &= 0.6 + 0.1\sin(5\pi t)\cos(2\pi x)\cos(2\pi y), \\ u &= \sin(3\pi t)\sin(2\pi x)\sin(2\pi y), \\ v &= \sin(\pi t)\sin(4\pi x)\sin(4\pi y), \end{aligned} \tag{33}$$

which satisfies (11) with additional source terms. The computational domain is $\Omega = (0, 1) \times (0, 1)$ and square quadrilateral elements are used. Table 2 shows the results of the LDG scheme for the two-dimensional isothermal NSK equations using piecewise linear and quadratic polynomials, indicating that the LDG discretization in Section 2.2 has optimal order of accuracy.

Table 1
Accuracy test of the LDG discretization for the one-dimensional isothermal NSK equations (1) with exact solution (31). The Van der Waals EOS is chosen as (3), $\theta = 0.85$, and the physical parameters in the isothermal NSK equations (1) are set as (32). The LDG discretization uses linear and quadratic basis functions and periodic boundary conditions. Results are for uniform meshes with M cells at time $t = 0.1$.

	M	$\|\rho - \rho_h\|_{L^2(\Omega)}$	Order	$\|u - u_h\|_{L^2(\Omega)}$	Order
P^1	16	1.65E−03	–	8.91E−03	–
	32	4.06E−04	2.03	2.27E−03	1.97
	64	1.08E−05	1.90	6.02E−04	1.92
	128	2.83E−05	1.94	1.56E−04	1.95
	256	7.25E−06	1.96	4.00E−05	1.97
P^2	16	1.21E−04	–	7.20E−04	–
	32	1.58E−05	2.95	9.64E−05	2.90
	64	2.18E−06	2.86	1.30E−05	2.90
	128	2.92E−07	2.90	1.70E−06	2.93
	256	3.81E−08	2.94	2.18E−07	2.96

Table 2
Accuracy test of the LDG discretization for the two-dimensional isothermal NSK equations (11) with exact solution (33). The Van der Waals EOS is chosen as (3), $\theta = 0.85$, and the physical parameters in the isothermal NSK equations (1) are set as (32). The LDG discretization uses piecewise linear and quadratic polynomials and periodic boundary conditions. Results are for uniform meshes with square elements at time $t = 0.1$.

	Mesh	$\|\rho - \rho_h\|_{L_2}$	Order	$\|u - u_h\|_{L_2}$	Order	$\|v - v_h\|_{L_2}$	Order
P^1	16×16	1.82E−03	–	3.95E−03	–	1.53E−02	–
	32×32	3.74E−04	1.85	9.42E−04	2.07	3.67E−03	2.06
	64×64	1.49E−04	1.95	2.36E−04	2.00	9.08E−04	2.01
	128×128	3.77E−05	1.98	5.91E−05	2.00	2.26E−04	2.00
P^2	16×16	3.38E−4	–	3.08E−4	–	1.81E−3	–
	32×32	3.35E−5	3.33	3.33E−5	3.21	2.22E−4	3.01
	64×64	3.85E−6	3.12	3.89E−6	3.10	2.81E−5	3.00
	128×128	4.80E−7	3.00	4.80E−7	3.02	3.51E−6	3.00

4.2.2. One-dimensional interface problem

As a further verification of the accuracy and robustness of the LDG discretization, we solve two traveling wave problems for the one-dimensional isothermal NSK equations. It is known that some numerical discretizations produce solutions with overshoots, or incorrect wave speeds at discontinuities for this test case, see e.g. [29]. First, we consider a stationary wave problem with initial conditions

$$\rho_0(x) = \frac{\rho_R + \rho_L}{2} + \frac{\rho_R - \rho_L}{2} \tanh\left(\frac{x - 0.5}{2}\sqrt{\mathbb{W}e}\right),$$
$$u_0(x) = \frac{u_R + u_L}{2} + \frac{u_R - u_L}{2} \tanh\left(\frac{x - 0.5}{2}\sqrt{\mathbb{W}e}\right). \tag{34}$$

The coefficients in the initial conditions (34) are taken as

$$(\rho_L, u_L) = (0.107, 0), \quad (\rho_R, u_R) = (0.602, 0).$$

We extend the domain $(0, 1)$ to $[-1, 1]$ with reflection symmetry at $x = 0$ and use periodic boundary conditions. The physical parameters in (11) are set as $\mathbb{R}e = 200$ and $\mathbb{W}e = 10\,000$ and the mesh contains 400 elements. We plot the solutions of the LDG scheme for the isothermal NSK equations with piecewise linear and quadratic polynomials at time $t = 0.1$ in Fig. 3. Fig. 3 shows that all numerical solutions are smooth without large oscillations, and the solutions resulting from linear and quadratic basis functions are indistinguishable at this mesh resolution. Since the initial condition is close to, but not exactly an equilibrium solution of the governing equations, the solution slightly changes in time and the velocity is small, but not equal to zero at the time shown in Fig. 3.

Next, we study a wave propagation problem. The initial conditions are set as (34) with

$$(\rho_R, u_R) = (0.107, 1.0), \quad (\rho_L, u_L) = (0.602, 1.0).$$

The LDG solution for the isothermal NSK equations with this initial condition results in a propagating traveling wave solution moving from the left to the right at speed 1.0. Again, stable numerical solutions are obtained as shown in Fig. 4.

4.2.3. Coalescence of two bubbles

An important test case is the simulation of the coalescence of two bubbles, which was also studied in [5,29]. The computational domain is $[0, 1]^2$. The parameters are $\mathbb{R}e = 512$, $\mathbb{W}e = 65\,500$. We consider two vapor bubbles of different radii, which are initially close to each other and at rest. The initial conditions are

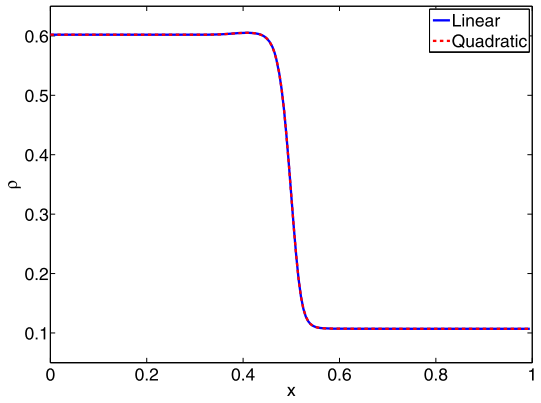

(a) density

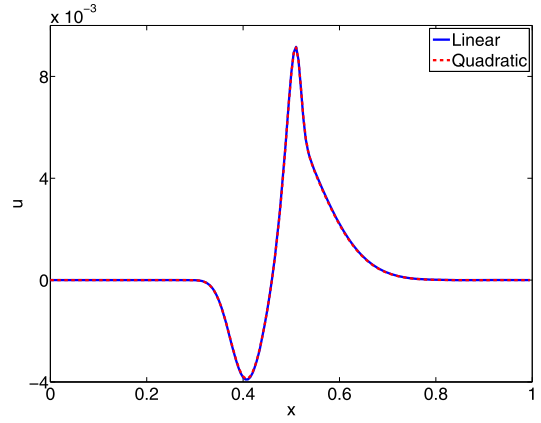

(b) velocity

Fig. 3. One-dimensional stationary wave problem. LDG solutions with piecewise linear and quadratic polynomials at $t = 0.1$ on a mesh containing 400 elements. The Van der Waals EOS is chosen as (3), $\theta = 0.85$, and the physical parameters in the isothermal NSK equations (1) are set as $\mathbb{R}e = 200$ and $\mathbb{W}e = 10\,000$.

$$\rho_0(\mathbf{x}) = \rho_1 + \frac{1}{2}(\rho_2 - \rho_1)\sum_{i=1}^{2}\tanh\left(\frac{(d_i(\mathbf{x}) - r_i)}{2}\sqrt{\mathbb{W}e}\right), \quad \mathbf{u} \equiv \mathbf{0}, \tag{35}$$

with ρ_1, ρ_2 close to an equilibrium given a fixed constant temperature. Here $d_i(\mathbf{x}) = \|\mathbf{x} - \mathbf{x}_i\|$ is the Euclidean distance and the points $\mathbf{x}_i$ are equal to $\mathbf{x}_1 = (0.4, 0.5)$ and $\mathbf{x}_2 = (0.78, 0.5)$, respectively. The radii of the two bubbles are $r_1 = 0.25$ and $r_2 = 0.1$. After some time, the bubbles will merge into one vapor bubble by capillarity and pressure forces.

Mass conservation and energy dissipation are critical parameters to investigate whether a numerical discretization for the NSK equations is suitable. To verify the mass conservation and energy dissipation properties of our LDG scheme, we denote the discrete mass and energy at time t, respectively, by

$$m_h(t) = \int_\Omega \rho_h(t)d\mathbf{x},$$

$$\mathcal{E}_h(t) = \int_\Omega \left(W(\rho_h(t)) + \frac{1}{2\mathbb{W}e}|\nabla\rho_h(t)|^2 + \frac{1}{2}\frac{|(\rho\mathbf{u})_h(t)|^2}{\rho_h(t)}\right)d\mathbf{x}.$$

The initial mass is $m_h(t_0) = \int_\Omega \rho_0(\mathbf{x})d\mathbf{x}$.

Before using the LDG discretization, we will discuss the mesh required for this method to capture the interface and to represent the solution accurately. For the isothermal NSK equations with equation of state (3), (30), we obtain the following results:

- Given the temperature $\theta = 0.85$, the critical densities are $\rho_v = 0.107$, $\rho_l = 0.602$. The interface width then is equal to

$$d = \frac{2(\rho_l - \rho_v)}{\sqrt{\Delta f_{max}}}\frac{1}{\sqrt{\mathbb{W}e}} = 14.04\frac{1}{\sqrt{\mathbb{W}e}}.$$

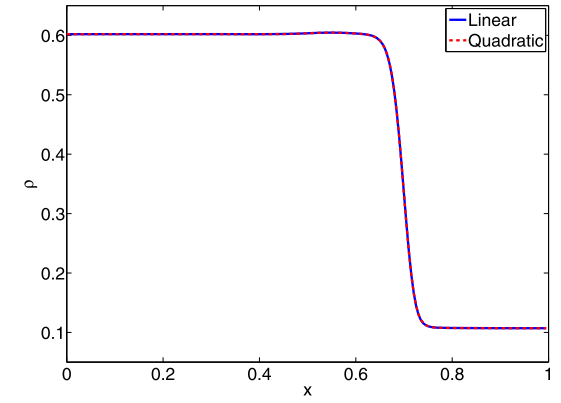

(a) density

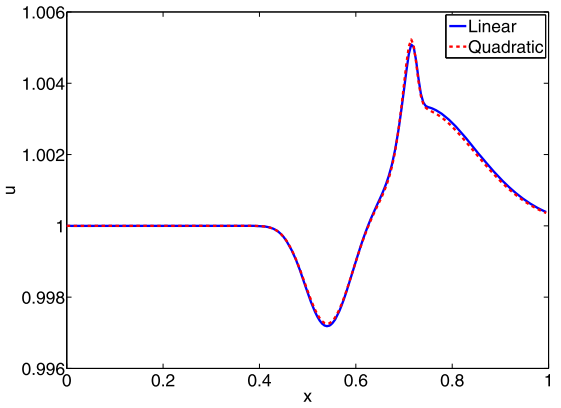

(b) velocity

Fig. 4. One-dimensional propagating wave problem. LDG solutions with piecewise linear and quadratic polynomials at $t = 0.2$ on a mesh containing 400 elements. The Van der Waals EOS is chosen as (3), $\theta = 0.85$, and the physical parameters in the isothermal NSK equations (1) are set as $\mathbb{R}e = 200$ and $\mathbb{W}e = 10\,000$.

Consequently $h = \frac{1}{\sqrt{\mathbb{W}e}}$ is a reasonable choice.

- Given the temperature $\theta = 0.8$, the critical densities are $\rho_v = 0.0800$, $\rho_l = 0.6442$. The interface width then is equal to

$$d = \frac{2(\rho_l - \rho_v)}{\sqrt{\Delta f_{max}}} \frac{1}{\sqrt{\mathbb{W}e}} = 12.00 \frac{1}{\sqrt{\mathbb{W}e}}.$$

Consequently $h = \frac{1}{\sqrt{\mathbb{W}e}}$ is a reasonable choice also for this case.

We use the LDG discretization with piecewise linear and quadratic polynomials for the isothermal NSK equations and the second order implicit Runge–Kutta time integration method (25) with stopping parameter $\eta_k = 10^{-6}$ in the Newton method. Given $\theta = 0.85$, the initial condition is set as (35) with $\rho_1 = 0.1$, $\rho_2 = 0.6$. We choose a mesh of 256^2 square elements. Fig. 5 presents the evolution for the mass loss and energy, showing that the mass is conserved, and the energy decreases monotonically in time. The evolution of the bubble coalescence process is shown in Figs. 6 and 7. These figures show that the two bubbles, which are below the critical temperature and initially close to each other and at rest, merge into one bubble during the simulation because of surface tension. After coalescence the resulting bubble slowly reaches an equilibrium state, in which the interface has a constant radius of curvature due to surface tension and the velocity field approaches zero.

The method for the isothermal NSK equations with $\theta = 0.85$ was also tested on a coarser mesh with 128^2 elements. Fig. 8 shows the density profiles at various times, indicating that stable results are still obtained on this coarser mesh. The density and pressure along the line $y = 0.5$ are displayed in Fig. 9, which shows that the diffuse interface has only 8 nodes in this test. The evolution of the energy is displayed in Fig. 10, showing that the energy is slightly increasing on a mesh with 128^2 elements for the isothermal NSK equations with $\mathbb{W}e = 65\,500$. On meshes coarser with less than 8 nodes in the diffuse interface no stable results are obtained for this Weber number.

Choosing $\theta = 0.8$, (29) results in critical densities $\rho_l = 0.6442$, $\rho_v = 0.0800$ with a larger density ratio. When the LDG discretization is applied to the isothermal NSK equations with $\theta = 0.8$ and initial condition (35) with $\rho_1 = 0.08$, $\rho_2 = 0.64$,

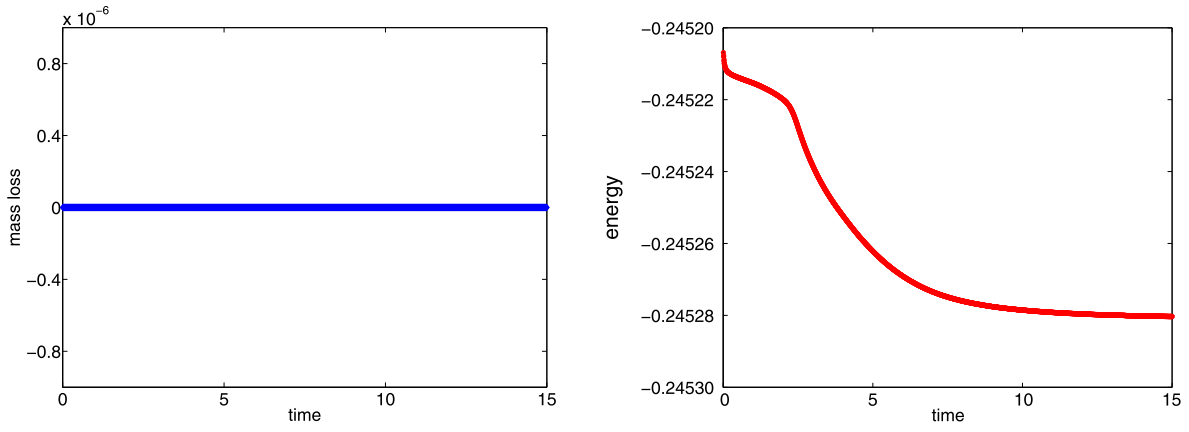

(a) mass loss (b) energy

Fig. 5. Evolution of mass loss and energy as a function of time during the coalescence of two bubbles computed with the LDG discretization of the isothermal NSK equations using piecewise linear polynomials on a mesh with 256^2 square elements. The Van der Waals EOS is chosen as (3), $\theta = 0.85$, and the physical parameters in the isothermal NSK equations (1) are set as $\mathbb{R}e = 512$, $\mathbb{W}e = 65\,500$. The initial condition is (35) with $\rho_1 = 0.1$, $\rho_2 = 0.6$.

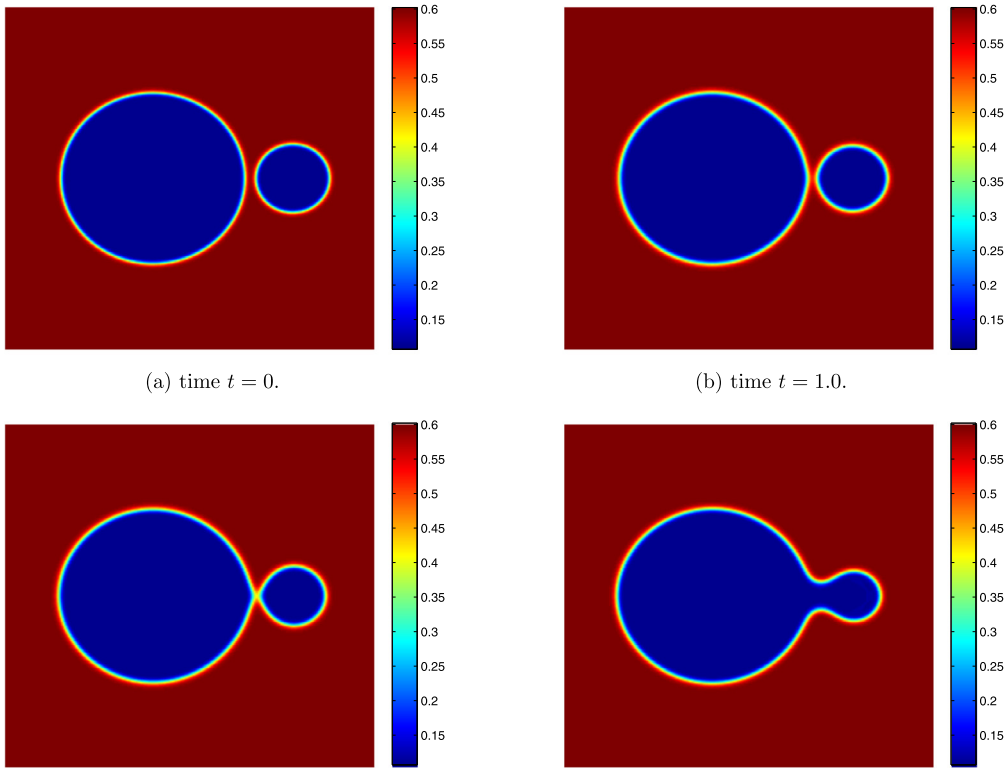

(a) time $t = 0.$ (b) time $t = 1.0.$

(c) time $t = 2.0.$ (d) time $t = 3.0.$

Fig. 6. Density ρ for two coalescing bubbles computed with the LDG discretization of the isothermal NSK equations using piecewise linear polynomials on a mesh with 256^2 square elements. The Van der Waals EOS is chosen as (3), $\theta = 0.85$, and the physical parameters in the isothermal NSK equations (1) are set as $\mathbb{R}e = 512$, $\mathbb{W}e = 65\,500$. The initial condition is (35) with $\rho_1 = 0.1$, $\rho_2 = 0.6$.

stable results are still obtained on a mesh of 256^2 elements, as can be seen from Fig. 12. Fig. 11 shows that the mass is conserved, and the energy is only slightly increasing in time.

We also study the behavior of the numerical scheme for the isothermal NSK equations when the initial densities are further away from the equilibrium densities ρ_l, ρ_v. For example, given a fixed temperature $\theta = 0.85$, $\rho_1 = 0.05$, $\rho_2 = 0.65$ were chosen in (35). We choose the parameters in (1) as $\mathbb{R}e = 500$, $\mathbb{W}e = 10\,000$, and the mesh of 100^2 elements. Mass and energy properties are presented in Fig. 13, which shows that the mass is conserved and the energy is decreasing in

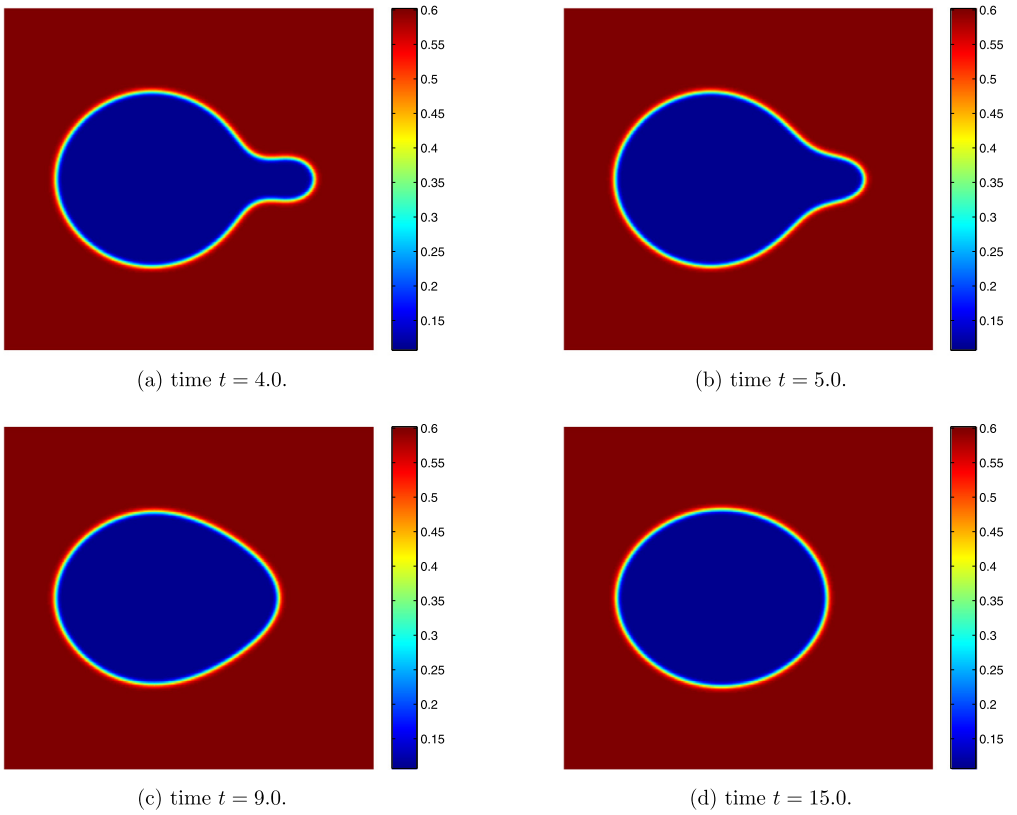

(a) time $t = 4.0$. (b) time $t = 5.0$.

(c) time $t = 9.0$. (d) time $t = 15.0$.

Fig. 7. Density ρ for two coalescing bubbles computed with the LDG discretization of the isothermal NSK equations using piecewise linear polynomials on a mesh with 256^2 square elements. The Van der Waals EOS is chosen as (3), $\theta = 0.85$, and the physical parameters in the isothermal NSK equations (1) are set as $\mathbb{R}e = 512$, $\mathbb{W}e = 65\,500$. The initial condition is (35) with $\rho_1 = 0.1$, $\rho_2 = 0.6$.

time. Fig. 14 shows the coalescence of bubbles for the isothermal NSK equations with $\mathbb{R}e = 200$, $\mathbb{W}e = 10\,000$ when the initial density is far away from an equilibrium on a mesh of 100^2 elements. Fig. 15 shows the results for the isothermal NSK equations with $\mathbb{R}e = 512$, $\mathbb{W}e = 65\,500$ when the initial density is far away from equilibrium on a mesh of 256^2 elements. Because of the non-equilibrium initial condition we get sound waves traveling to the boundaries of the domain and transported back into the domain on the opposite side due to the periodic boundary conditions. For the isothermal NSK equations with $\mathbb{R}e = 512$, $\mathbb{W}e = 65\,500$ on a mesh of 256^2 elements, the amplitude of these sound waves is so large that this results in regions where the density is so low that a bubble occurs there. Since the simulations are isothermal, there is no latent heat that prevents this. The large Weber number also helps the formation of a bubble, since the surface tension is rather low.

4.3. Numerical experiments for the non-isothermal NSK equations

Choosing the temperature $\theta = 0.989$ and the Van der Waals equation of state (8), the Maxwell states are

$$\rho_v = 0.79525689, \quad \rho_l = 1.21357862. \tag{36}$$

4.3.1. Accuracy test

For the accuracy test of the LDG discretization of the one-dimensional non-isothermal NSK equations (6), a smooth exact solution is chosen as

$$\begin{cases} \rho(x,t) = 0.6 + 0.1\sin(5\pi t)\cos(2\pi x), \\ v(x,t) = \sin(3\pi t)\sin(2\pi x), \\ \theta(x,t) = 0.8 + 0.1\sin(\pi t)\sin(2\pi x), \end{cases} \tag{37}$$

which satisfies the non-isothermal NSK equations (6) with a properly chosen source term $\mathbf{S}$. The Prandtl number $\mathbb{P}r$ in (6) is chosen as $\mathbb{P}r = 0.843$, and $C_v = 5.375$.

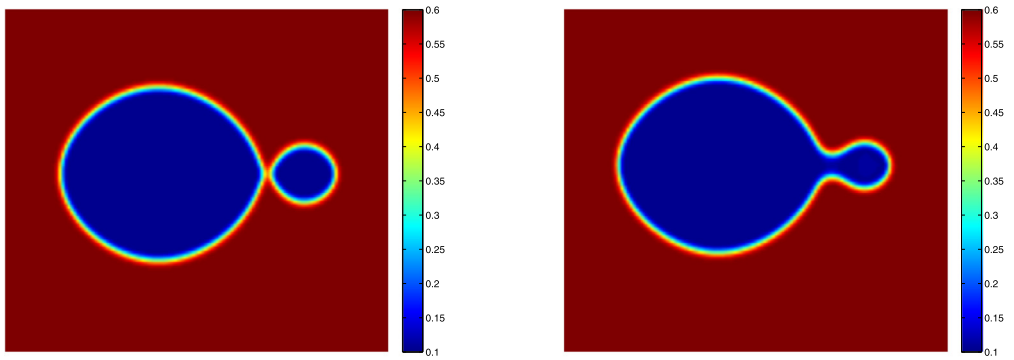

(a) t=2.0 (b) t=3.0

(c) t=4.0 (d) t=5.0

Fig. 8. Density ρ for two coalescing bubbles computed with the LDG discretization of the isothermal NSK equations using piecewise linear polynomials on a mesh with 128^2 square elements. The Van der Waals EOS is chosen as (3), $\theta = 0.85$, and the physical parameters in the isothermal NSK equations (1) are set as $\mathbb{R}e = 512$, $\mathbb{W}e = 65\,500$. The initial condition is (35) with $\rho_1 = 0.1$, $\rho_2 = 0.6$.

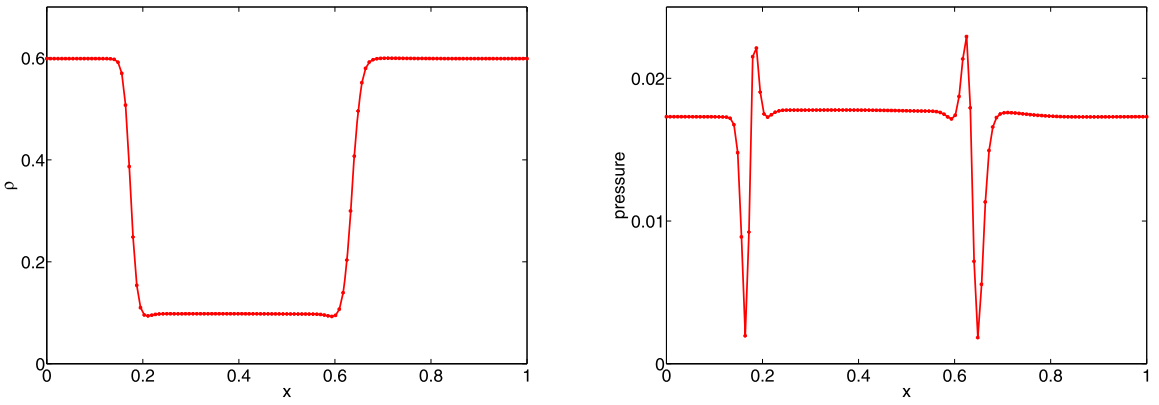

(a) density along $y = 0.5$ (b) pressure along $y = 0.5$

Fig. 9. Density and pressure along $y = 0.5$ at time $t = 5.0$ for the coalescence of two bubbles for the isothermal NSK equations using piecewise linear polynomials on a mesh with 128^2 square elements. The Van der Waals EOS is chosen as (3), $\theta = 0.85$, and the physical parameters in the isothermal NSK equations (1) are set as $\mathbb{R}e = 512$, $\mathbb{W}e = 65\,500$. The initial condition is (35) with $\rho_1 = 0.1$, $\rho_2 = 0.6$.

In order to verify the accuracy of the LDG scheme for the two-dimensional non-isothermal NSK equations (6), we select the exact smooth solution

$$\begin{cases} \rho(x,t) = 0.6 + 0.1\sin(5\pi t)\cos(2\pi x)\cos(2\pi y), \\ u(x,t) = \sin(3\pi t)\sin(2\pi x)\sin(2\pi y), \\ v(x,t) = \sin(3\pi t)\sin(4\pi x)\sin(4\pi y), \\ \theta(x,t) = 0.8 + 0.1\sin(\pi t)\sin(2\pi x)\cos(2\pi y), \end{cases} \tag{38}$$

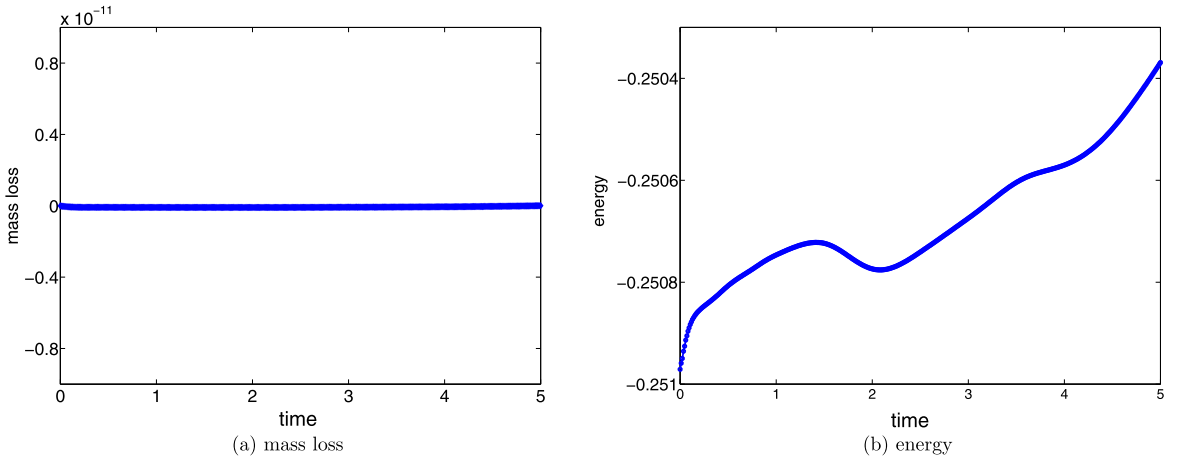

(a) mass loss (b) energy

Fig. 10. Evolution of mass loss and energy as a function of time during the coalescence of two bubbles computed with the LDG discretization of the isothermal NSK equations using piecewise linear polynomials on a mesh with 128^2 square elements. The Van der Waals EOS is chosen as (3), $\theta = 0.85$ and the physical parameters in the isothermal NSK equations (1) are set as $\mathbb{R}e = 512$, $\mathbb{W}e = 65\,500$. The initial condition is (35) with $\rho_1 = 0.1$, $\rho_2 = 0.6$.

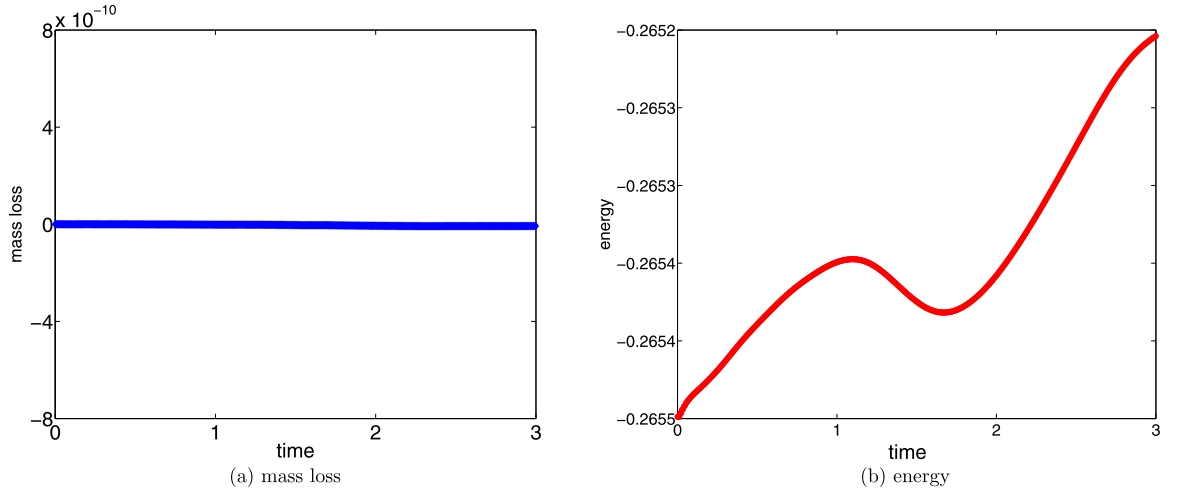

(a) mass loss (b) energy

Fig. 11. Evolution of mass loss and energy as a function of time during the simulation of two bubbles for the isothermal NSK equations with $\mathbb{R}e = 512$, $\mathbb{W}e = 65\,500$ on a mesh of 256^2 elements using piecewise linear polynomials.The Van der Waals EOS is chosen as (3), $\theta = 0.8$. The initial condition is (35) with $\rho_1 = 0.08$, $\rho_2 = 0.64$.

Table 3
Accuracy test of the LDG discretization for the one-dimensional non-isothermal NSK equations (6) with exact solution (37). The physical parameters are chosen as $\mathbb{R}e = 50$, $\mathbb{W}e = 1000$, $\mathbb{P}r = 0.843$, $C_v = 5.375$, and the Van der Waals EOS is set as (8). LDG discretization with piecewise linear and quadratic polynomials, periodic boundary conditions, uniform meshes and time $t = 0.1$.

	Mesh	$\|\rho - \rho_h\|_{L_2}$	Order	$\|u - u_h\|_{L_2}$	Order	$\|\theta - \theta_h\|_{L_2}$	Order
P^1	16	1.43E−03	–	3.65E−03	–	2.88E−04	–
	32	3.551E−04	2.01	9.32E−04	1.97	7.44E−05	1.95
	64	8.89E−05	2.00	2.36E−04	1.98	1.90E−05	1.97
	128	2.22E−05	2.00	5.96E−05	1.99	4.80E−06	1.99
	256	5.56E−06	2.00	1.50E−05	1.99	1.20E−06	2.00
P^2	16	2.71E−5	–	1.35E−4	–	1.21E−5	–
	32	2.14E−6	3.66	1.71E−-5	2.68	1.33E−6	3.18
	64	2.42E−7	3.14	2.18E−6	2.97	1.54E−7	3.11
	128	2.96E−8	3.03	2.77E−7	2.98	1.86E−8	3.04
	256	3.70E−9	3.00	3.50E−8	2.96	2.31E−9	3.01

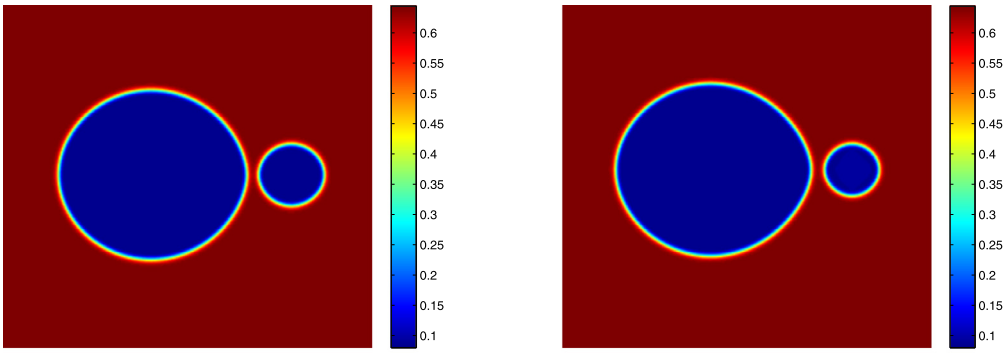

(a) time $t = 1$. (b) time $t = 2$.

(c) time $t = 2.5$. (d) time $t = 3$.

Fig. 12. Density ρ for two bubbles computed with the LDG discretization of the isothermal NSK equations with $\mathbb{R}e = 512$, $\mathbb{W}e = 65\,500$ on a mesh of 256^2 elements using piecewise linear polynomials. The Van der Waals EOS is chosen as (3), $\theta = 0.8$. The initial condition is (35) with $\rho_1 = 0.08$, $\rho_2 = 0.64$.

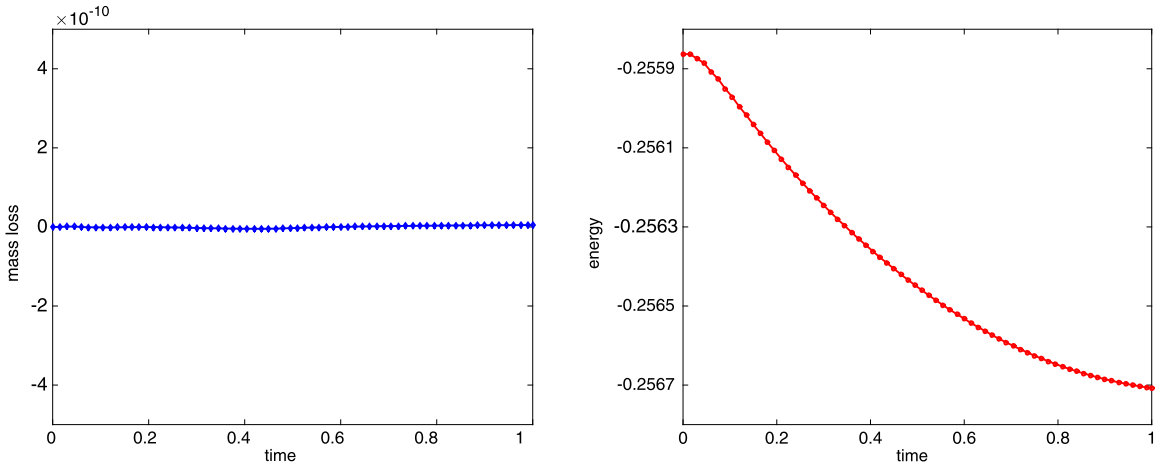

(a) mass loss (b) energy

Fig. 13. Evolution of mass loss and energy as a function of time during the coalescence of two bubbles computed with the LDG discretization of the isothermal NSK equations with $\mathbb{R}e = 200$, $\mathbb{W}e = 10\,000$ on a mesh with 100^2 square elements. Piecewise linear polynomials are used. The Van der Waals EOS is chosen as (3), $\theta = 0.85$. The initial condition is (35) with $\rho_1 = 0.05$, $\rho_2 = 0.65$.

which satisfies the non-isothermal NSK equations (6) with a properly chosen source term. The results of the accuracy tests of the LDG discretization for the 1D and 2D non-isothermal NSK equations are given in Tables 3 and 4, respectively. From these results, we can see that the LDG discretization for the non-isothermal NSK equations has optimal order of accuracy.

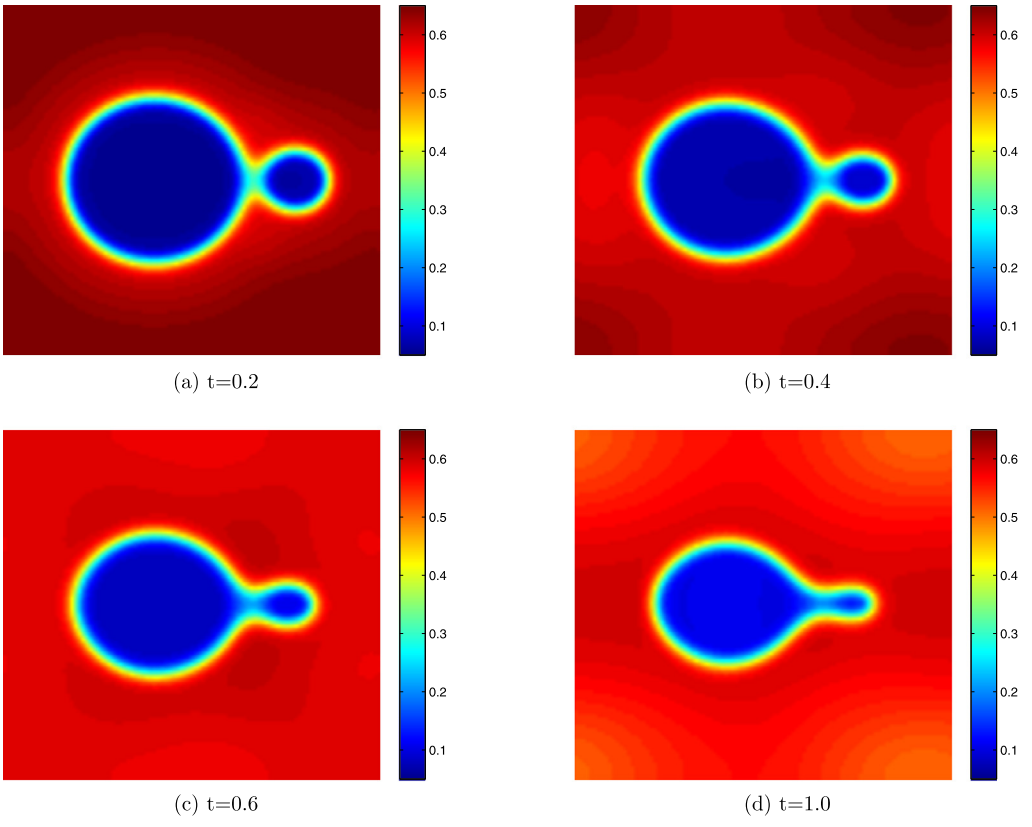

Fig. 14. Coalescence of two bubbles for the isothermal NSK equations with $\mathbb{R}e = 200$, $\mathbb{W}e = 10\,000$ on a mesh of 100^2 elements. Piecewise linear polynomials are used. The Van der Waals EOS is chosen as (3), $\theta = 0.85$. The initial condition is (35) with $\rho_1 = 0.05$, $\rho_2 = 0.65$.

Table 4
Accuracy test of the LDG discretization for the two-dimensional non-isothermal NSK equations (6) with exact solution (38). The physical parameters are chosen as $\mathbb{R}e = 50$, $\mathbb{W}e = 1000$, $\mathbb{P}r = 0.843$, $C_v = 5.375$, and the Van der Waals EOS is set as (8). LDG discretization with piecewise linear and quadratic polynomials, periodic boundary conditions, and uniform meshes with square elements at time $t = 0.1$.

	Mesh	$\|\rho - \rho_h\|_{L_2}$	Order	$\|u - u_h\|_{L_2}$	Order	$\|\theta - \theta_h\|_{L_2}$	Order
P^1	16×16	2.08E−03	–	3.72E−02	–	9.85E−4	–
	32×32	5.61E−04	1.88	9.36E−04	1.99	2.63E−4	1.90
	64×64	1.47E−04	1.94	2.34E−04	2.00	6.91E−5	1.94
	128×128	3.76E−05	1.97	5.85E−05	2.00	1.76E−5	1.97
P^2	16×16	5.11E−4	–	6.66E−4	–	7.36E−4	–
	32×32	5.57E−5	3.19	6.94E−5	3.21	1.28E−4	2.51
	64×64	6.93E−6	3.01	7.99E−6	3.11	1.56E−5	3.04
	128×128	8.74E−7	2.98	9.70E−7	3.04	1.78E−6	3.13

4.3.2. One-dimensional interface problem

In this section we consider a one-dimensional interface problem to investigate the accuracy and robustness of the LDG discretization of the non-isothermal NSK equations. The initial conditions are set as a similar form as (34) with

$$(\rho_L, u_L, \theta_L) = (0.795, 0.0, 0.989), \quad (\rho_R, u_R, \theta_R) = (1.213, 0.0, 0.989). \tag{39}$$

The domain is $[-5, 5]$.

Fig. 16 shows that the LDG scheme for the non-isothermal NSK equations results in accurate and stable solutions. Fig. 17 compares the LDG solutions for the isothermal and non-isothermal NSK equations with the Van der Waals equation of state (8). The dimensionless numbers are equal to $\mathbb{R}e = 128.6$, $\mathbb{W}e = 968.6$ and the initial conditions are defined in (39). Fig. 17 shows that, compared to the isothermal NSK equations, the LDG solutions for the non-isothermal NSK equations result in less oscillations in the density near the interface.

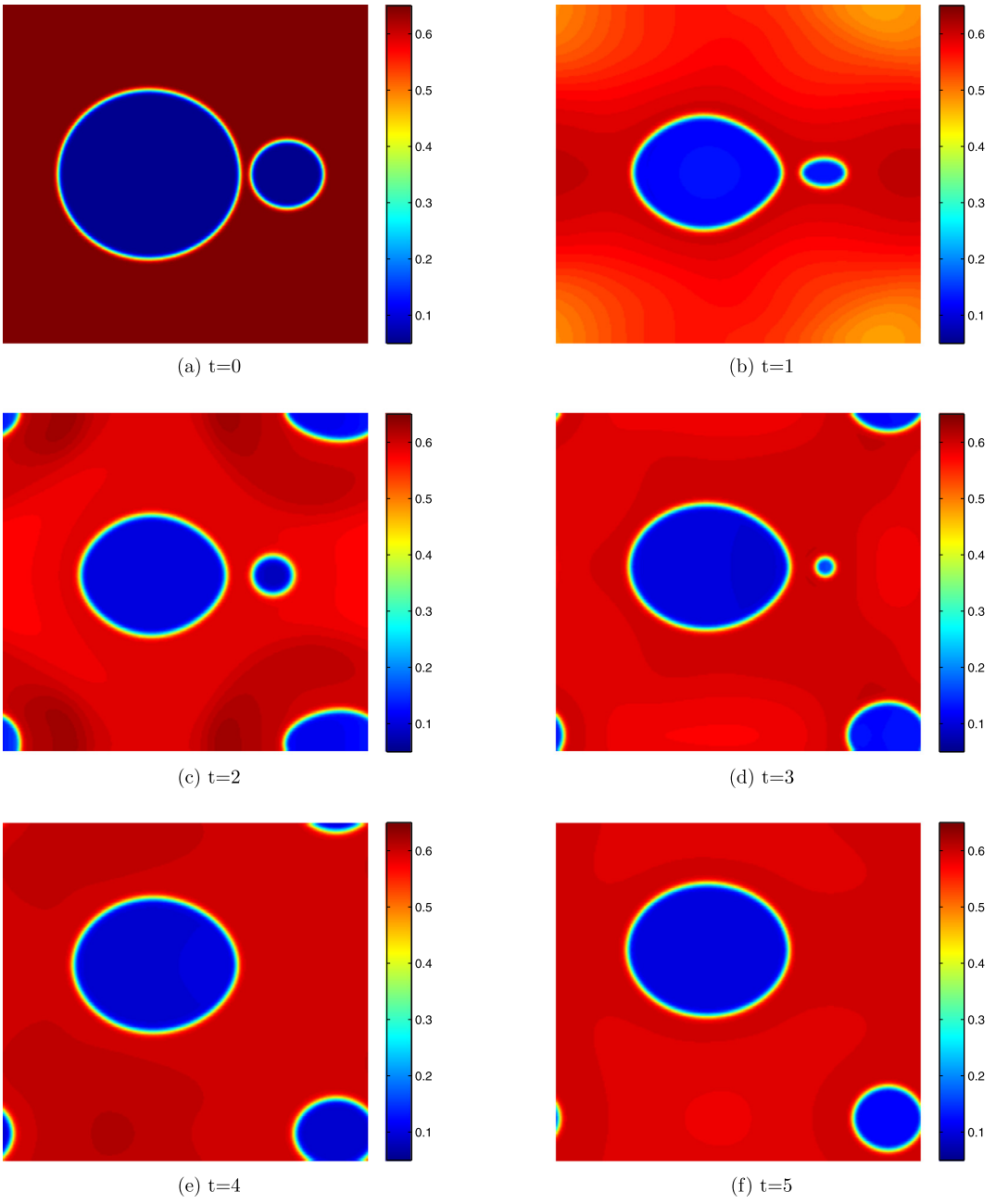

Fig. 15. Coalescence of two bubbles for the isothermal NSK equations with $\mathbb{R}e = 512$, $\mathbb{W}e = 65\,500$ on a mesh of 256^2 elements. Piecewise linear polynomials are used. The Van der Waals EOS is chosen as (3), $\theta = 0.85$. The initial condition is (35) with $\rho_1 = 0.05$, $\rho_2 = 0.65$.

4.3.3. Coalescence of two bubbles

Next, we simulate the coalescence of two bubbles. The parameters are $\mathbb{R}e = 950$, $\mathbb{W}e = 34\,455$. The computational domain is $[0, 1]^2$. We consider two vapor bubbles of different radii, which are initially close to each other and at rest. The initial conditions are

$$\rho_0(\mathbf{x}) = \rho_1 + \frac{1}{2}(\rho_2 - \rho_1)\sum_{i=1}^{2}\tanh\left(\frac{(d_i(\mathbf{x}) - r_i)}{2}\sqrt{\mathbb{W}e}\right), \quad \mathbf{u} \equiv \mathbf{0}, \quad \theta = \theta_0 \tag{40}$$

where θ_0 is a chosen constant, and ρ_1, ρ_2 are constants close to the critical densities for given θ_0. These values will be specified in each test. The points $\mathbf{x}_i$ are equal to $\mathbf{x}_1 = (0.4, 0.5)$ and $\mathbf{x}_2 = (0.78, 0.5)$. The radii of the two bubbles are $r_1 = 0.25$ and $r_2 = 0.1$.

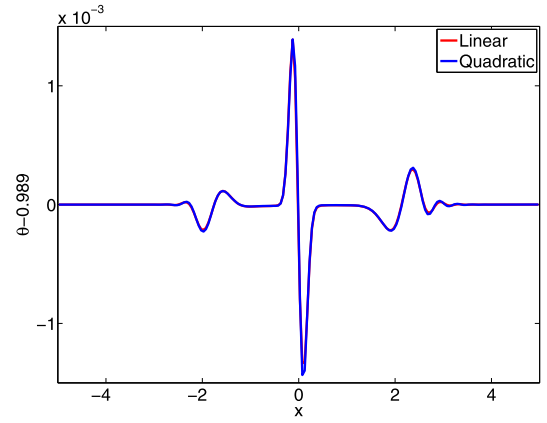

(a) $\theta - 0.989$

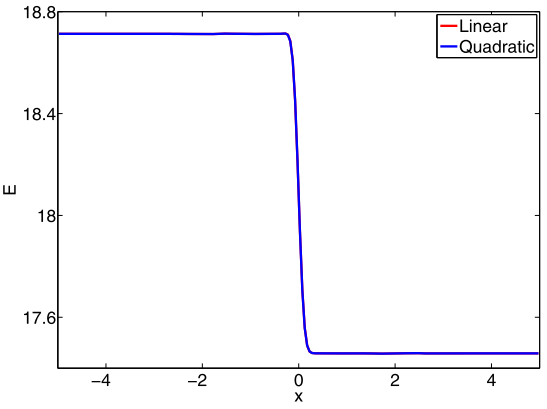

(b) Energy

Fig. 16. One-dimensional static interface problem for the non-isothermal NSK equations. Numerical solutions obtained with the LDG scheme with piecewise quadratic polynomials at $t = 2.0$ on a mesh containing 400 elements. The physical parameters are chosen as $\mathbb{R}e = 128.6$, $\mathbb{W}e = 968.6$, $\mathbb{P}r = 0.843$, $C_v = 5.375$, and the Van der Waals EOS is set as (8).

For the non-isothermal NSK equations with equation of state (8), the interface width (30) shows the following results:

- Given the initial temperature $\theta = 0.989$, the critical densities are $\rho_v = 0.7952$, $\rho_l = 1.2135$, and the interface width follows as

$$d = \frac{2(\rho_l - \rho_v)}{\sqrt{\Delta f_{max}}} \frac{1}{\sqrt{\mathbb{W}e}} = 31.05 \frac{1}{\sqrt{\mathbb{W}e}}.$$

  Then the mesh size $h = \frac{2}{\sqrt{\mathbb{W}e}}$ can be chosen.
- Given the initial temperature $\theta = 0.95$, the critical densities are $\rho_v = 0.5790$, $\rho_l = 1.4617$, and the interface width follows as

$$d = \frac{2(\rho_l - \rho_v)}{\sqrt{\Delta f_{max}}} \frac{1}{\sqrt{\mathbb{W}e}} = 14.42 \frac{1}{\sqrt{\mathbb{W}e}}.$$

  Then the mesh size $h = \frac{1}{\sqrt{\mathbb{W}e}}$ is a reasonable choice.

We use the LDG discretization for the non-isothermal NSK equations with bi-linear basis functions and the second order implicit Runge–Kutta time integration method (25) with stopping parameter $\eta_k = 10^{-6}$ in (28). Similar to the isothermal case, the bubbles merge into one vapor bubble, which tends to be of circular shape later in time by capillarity and pressure forces. Choosing $\theta_0 = 0.989$, the initial condition is set as (40) with $\rho_1 = 0.795$, $\rho_2 = 1.213$. The LDG discretizations is used for the non-isothermal NSK equations with $\mathbb{W}e = 34\,455$ on a mesh of 200^2 square elements and a mesh of 100^2 square elements. These two meshes lead to very similar results for mass conservation and entropy increase, see Fig. 18. The process of coalescence computed for the non-isothermal NSK equations with initial condition (40) and $\rho_1 = 0.795$,

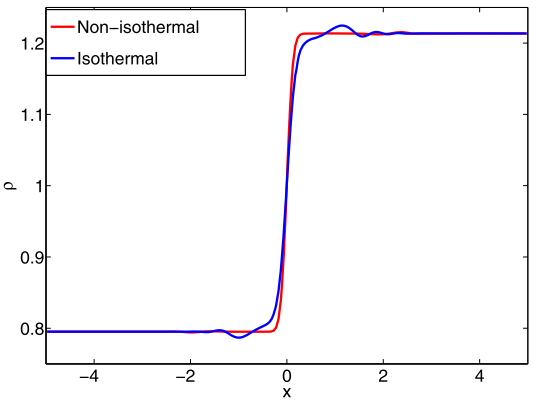

(a) density

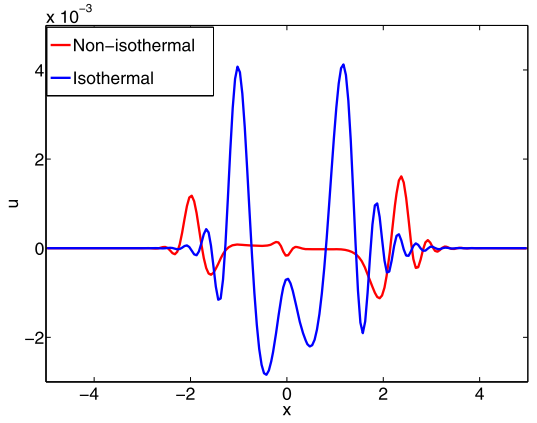

(b) velocity

Fig. 17. One-dimensional static interface problem for the isothermal and non-isothermal NSK equations, numerical solutions obtained with the piecewise quadratic polynomials at $t = 2.0$ on a mesh containing 400 elements. The physical parameters are chosen as $\mathbb{R}e = 128.6$, $\mathbb{W}e = 968.6$, $\mathbb{P}r = 0.843$, $C_v = 5.375$, and the Van der Waals EOS is set as (8).

$\rho_2 = 1.213$, $\theta_0 = 0.989$ on a mesh of 200^2 elements is shown in Figs. 19–21. Density and pressure along the line $y = 0.5$ for two coalescing bubbles are computed with the LDG discretization of the non-isothermal NSK equations on a mesh with 100^2 square elements, shown in Fig. 22.

Given $\theta_0 = 0.95$, critical densities $\rho_v = 0.5790$, $\rho_l = 1.4617$ with a larger density ratio are found by (29) with equations of state (8). The initial condition is set as (40) with $\rho_1 = 0.579$, $\rho_2 = 1.462$ and $\theta_0 = 0.95$. The time evolution of the bubbles, mass and entropy are shown in Figs. 23 and 25. The mass is conserved, and the entropy is a non-decreasing function of time apart from a small interval in which it is almost constant. For $\theta_0 = 0.92$, the critical densities are $\rho_v = 0.479$, $\rho_l = 1.587$. The initial condition is set as (40) with $\rho_1 = 0.479$, $\rho_2 = 1.587$. Fig. 24 shows that stable results are obtained although the entropy does not increase during part of the calculation. A finer mesh is required to guarantee an increasing entropy in this case.

The behavior of the numerical scheme for the Non-isothermal NSK equations is also studied when the initial densities are further away from the equilibrium densities ρ_l, ρ_v. Given $\theta_0 = 0.989$, $\rho_1 = 0.6, \rho_2 = 1.4$ is set in (40). Fig. 26 shows the mass is conserved and entropy is increasing in time. Fig. 27 shows the momentum in both directions and energy are conserved. Fig. 28 presents the coalescence, similar results with Fig. 19.

5. Conclusions

We developed local discontinuous Galerkin methods for the solution of the (non)-isothermal Navier–Stokes–Korteweg equations containing the Van der Waals equation of state and nonlinear third order density derivatives. The LDG methods are based on the conservative form of the NSK equations and are relatively simple compared to other available numerical discretizations for the NSK equations. A diagonally implicit Runge–Kutta integration time method is used to integrate in time in order to deal with the severe time step restriction encountered for explicit time integration methods. The Jacobian matrix for the implicit Runge–Kutta method includes the extra variables for the higher order derivatives. The numerical experiments demonstrate the capabilities, accuracy and stability of the proposed LDG discretizations of the NSK equations.

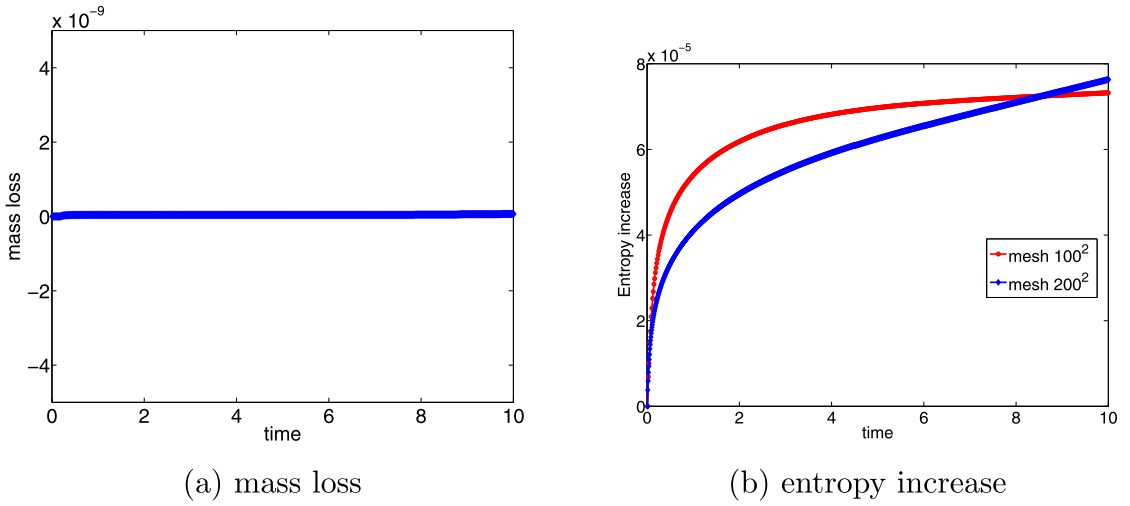

(a) mass loss (b) entropy increase

Fig. 18. Evolution of mass loss on a mesh of 100^2 elements and entropy on meshes of 100^2 and 200^2 square elements as a function of time during the coalescence of two bubbles for the non-isothermal NSK equations with $\mathbb{R}e = 950$, $\mathbb{W}e = 34455$, $\mathbb{P}r = 0.843$, $C_v = 5.375$. The initial condition is set as (40) with $\rho_1 = 0.795$, $\rho_2 = 1.213$ and $\theta_0 = 0.989$.

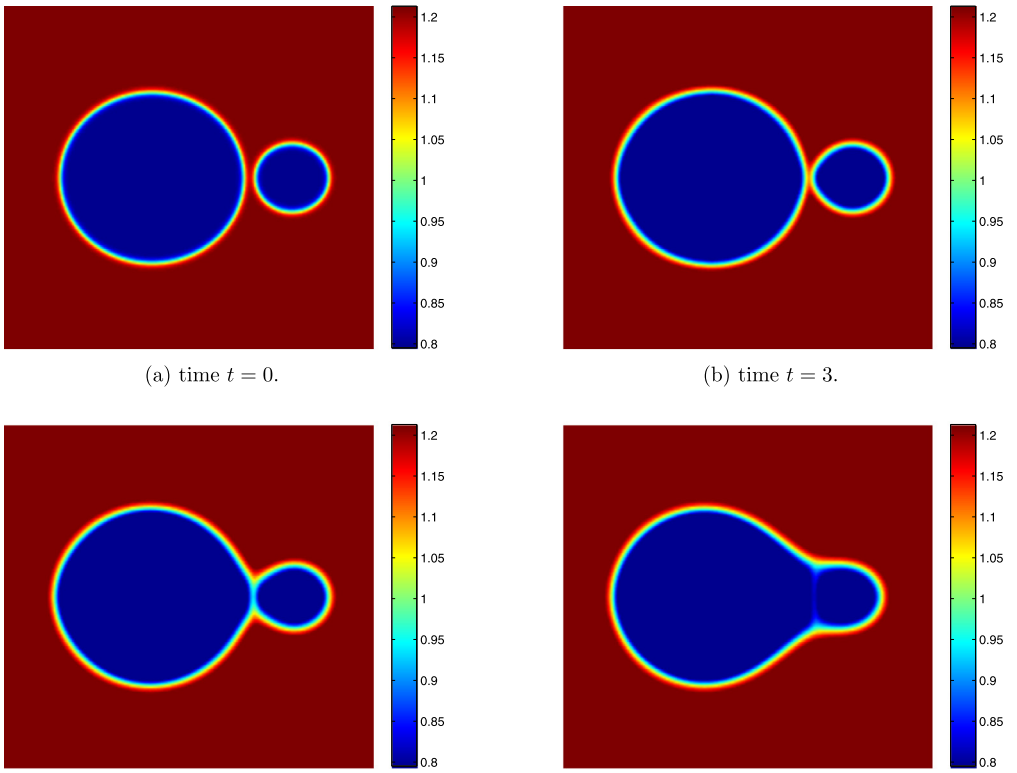

(a) time $t = 0$. (b) time $t = 3$.

(c) time $t = 6$. (d) time $t = 9$.

Fig. 19. Density ρ for two coalescing bubbles computed with the LDG discretization of the non-isothermal NSK equations using piecewise linear polynomials on a mesh with 200^2 square elements. The physical parameters are chosen as $\mathbb{R}e = 950$, $\mathbb{W}e = 34455$, $\mathbb{P}r = 0.843$, $C_v = 5.375$, and the Van der Waals EOS is set as (8). The initial condition is set as (40) with $\rho_1 = 0.795$, $\rho_2 = 1.213$ and $\theta_0 = 0.989$.

It is worthwhile to point out that the proposed LDG discretization is straightforward and works well for larger density ratios, but has limitations in the mesh required to obtain stable solutions and the correct energy or entropy behavior.

In future research we will also consider the (non-)isothermal NSK equations for initial conditions that result in a larger elliptic region in the phase transition area. This will be combined with local mesh refinement to capture the interface more efficiently.

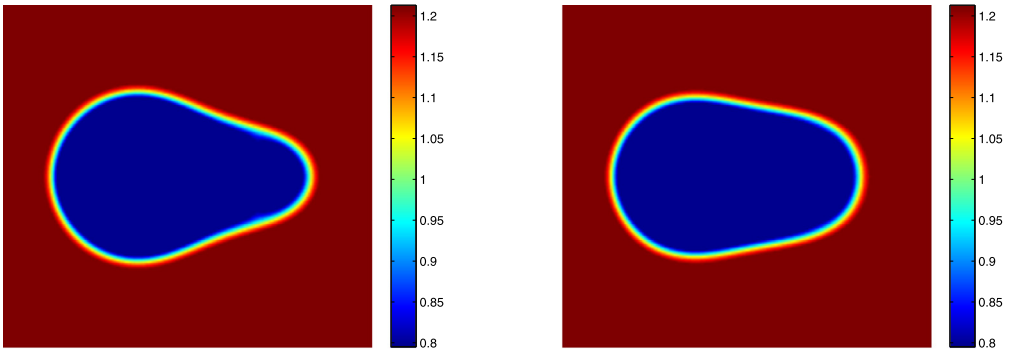

(a) time $t = 12$. (b) time $t = 15$.

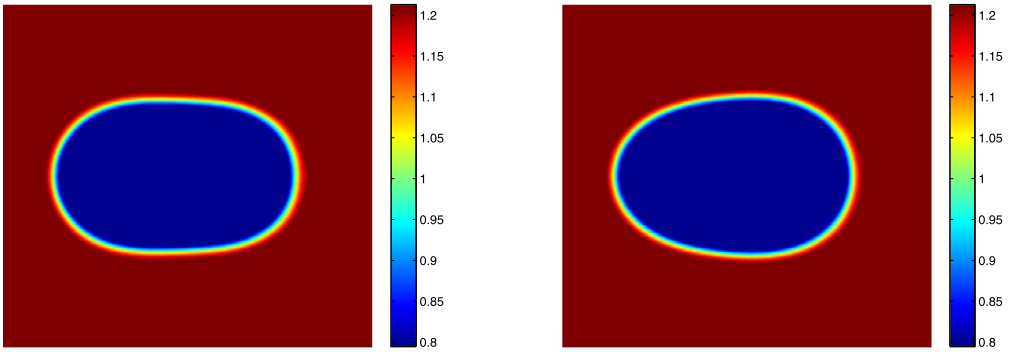

(c) time $t = 18$. (d) time $t = 21$.

Fig. 20. Density ρ for two coalescing bubbles computed with the LDG discretization of the non-isothermal NSK equations using piecewise linear polynomials with 200^2 square elements. The physical parameters are chosen as $\mathbb{R}e = 950$, $\mathbb{W}e = 34455$, $\mathbb{P}r = 0.843$, $C_v = 5.375$, and the Van der Waals EOS is set as (8). The initial condition is set as (40) with $\rho_1 = 0.795$, $\rho_2 = 1.213$ and $\theta_0 = 0.989$.

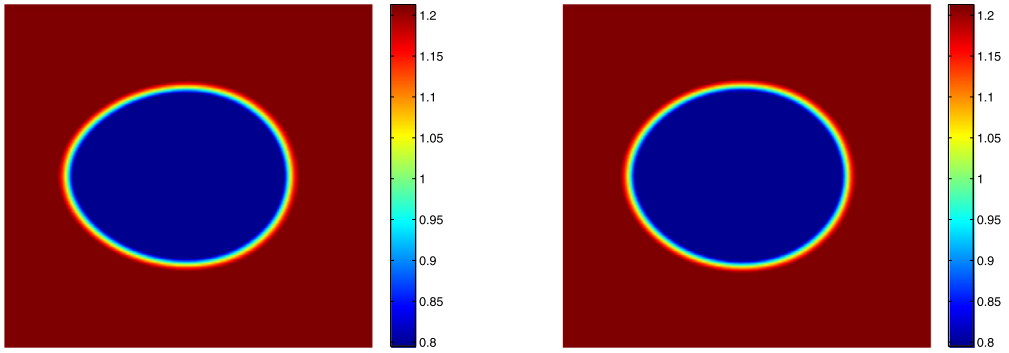

(a) time $t = 28$. (b) time $t = 30$.

Fig. 21. Density ρ for two coalescing bubbles computed with an LDG discretization of the non-isothermal NSK equations using piecewise linear polynomials functions with 200^2 square elements. The physical parameters are chosen as $\mathbb{R}e = 950$, $\mathbb{W}e = 34455$, $\mathbb{P}r = 0.843$, $C_v = 5.375$, and the Van der Waals EOS is set as (8). The initial condition is set as (40) with $\rho_1 = 0.795$, $\rho_2 = 1.213$ and $\theta_0 = 0.989$.

Acknowledgements

L. Tian acknowledges the China Scholarship Council (CSC), grant No. 2011634101, for giving the opportunity and financial support to study at the University of Twente in the Netherlands. Research of Yan Xu is supported by NSFC grants Nos. 11371342, 11031007, Fok Ying Tung Education Foundation No. 131003. Research of J.J.W. van der Vegt was partially supported by the High-end Foreign Experts Recruitment Program (GDW201371001 68), while the author was in residence at the University of Science and Technology of China in Hefei, Anhui, China.

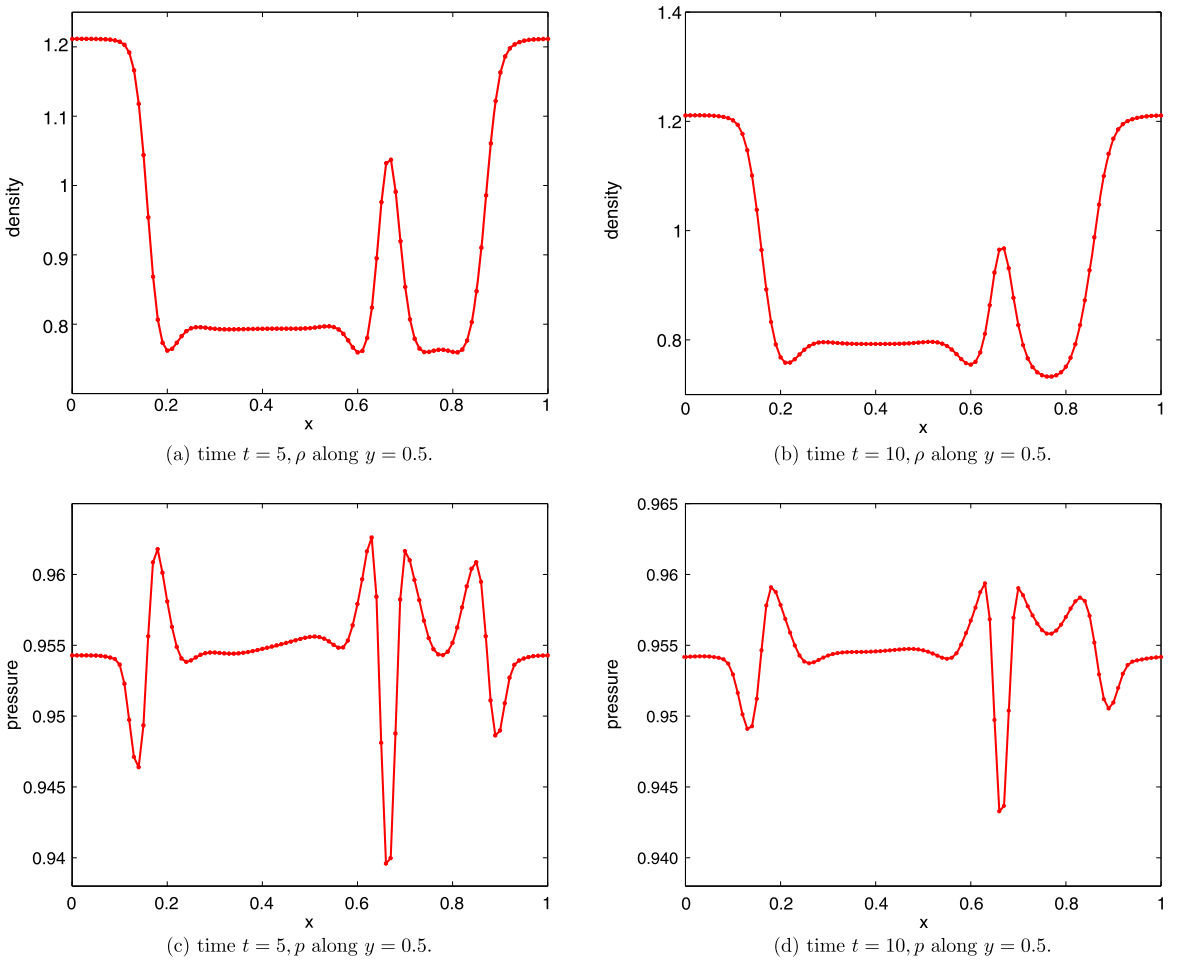

(a) time $t = 5, \rho$ along $y = 0.5$.

(b) time $t = 10, \rho$ along $y = 0.5$.

(c) time $t = 5, p$ along $y = 0.5$.

(d) time $t = 10, p$ along $y = 0.5$.

Fig. 22. Density and pressure along $y = 0.5$ for two coalescing bubbles computed with the LDG discretization of the non-isothermal NSK equations using piecewise linear polynomials on a mesh with 100^2 square elements. The physical parameters are chosen as $\mathbb{R}e = 950$, $\mathbb{W}e = 34\,455$, $\mathbb{P}r = 0.843$, $C_v = 5.375$, and the Van der Waals EOS is set as (8). The initial condition is set as (40) with $\rho_1 = 0.795$, $\rho_2 = 1.213$ and $\theta_0 = 0.989$.

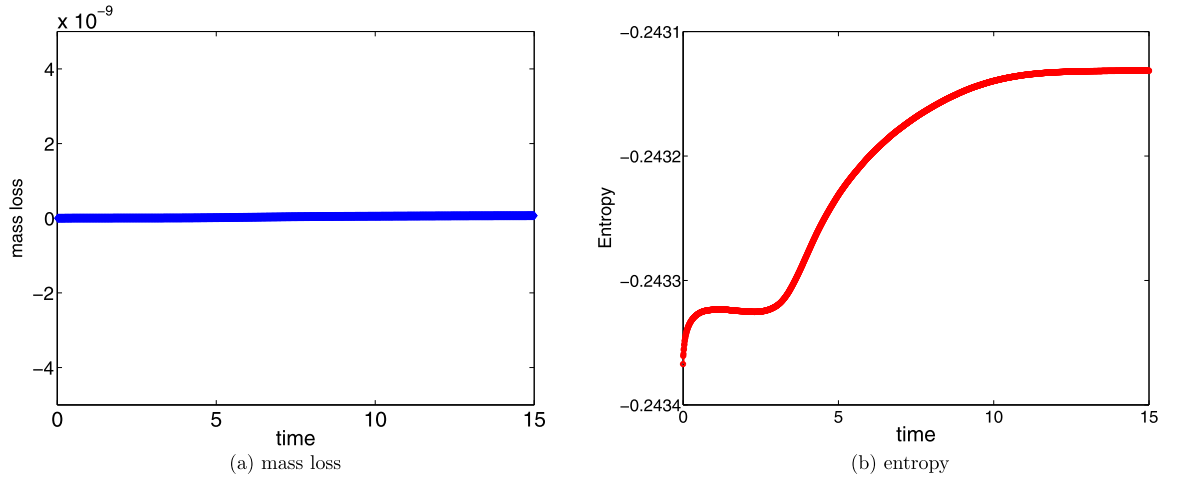

(a) mass loss

(b) entropy

Fig. 23. Evolution of mass loss and entropy as a function of time during the coalescence of two bubbles for the non-isothermal NSK equations, the initial temperature set as $\theta = 0.95$, a mesh of 200^2 square elements. The physical parameters are chosen as $\mathbb{R}e = 950$, $\mathbb{W}e = 34\,455$, $\mathbb{P}r = 0.843$, $C_v = 5.375$, and the Van der Waals EOS is set as (8). The initial condition is set as (40) with $\rho_1 = 0.579$, $\rho_2 = 1.462$ and $\theta_0 = 0.95$.

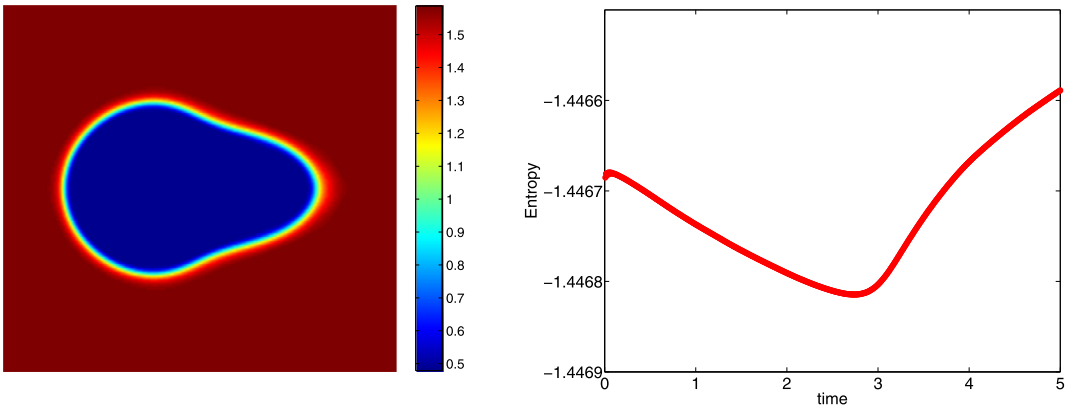

(a) t=5 (b) Entropy

Fig. 24. Density profile at $t = 5.0$ and entropy as a function of time during the coalescence of two bubbles for the non-isothermal NSK equations, the initial temperature set as $\theta = 0.92$, a mesh of 200^2 square elements. The physical parameters are chosen as $\mathbb{R}e = 950$, $\mathbb{W}e = 34\,455$, $\mathbb{P}r = 0.843$, $C_v = 5.375$, and the Van der Waals EOS is set as (8). The initial condition is set as (40) with $\rho_1 = 0.479$, $\rho_2 = 1.587$, $\theta_0 = 0.92$.

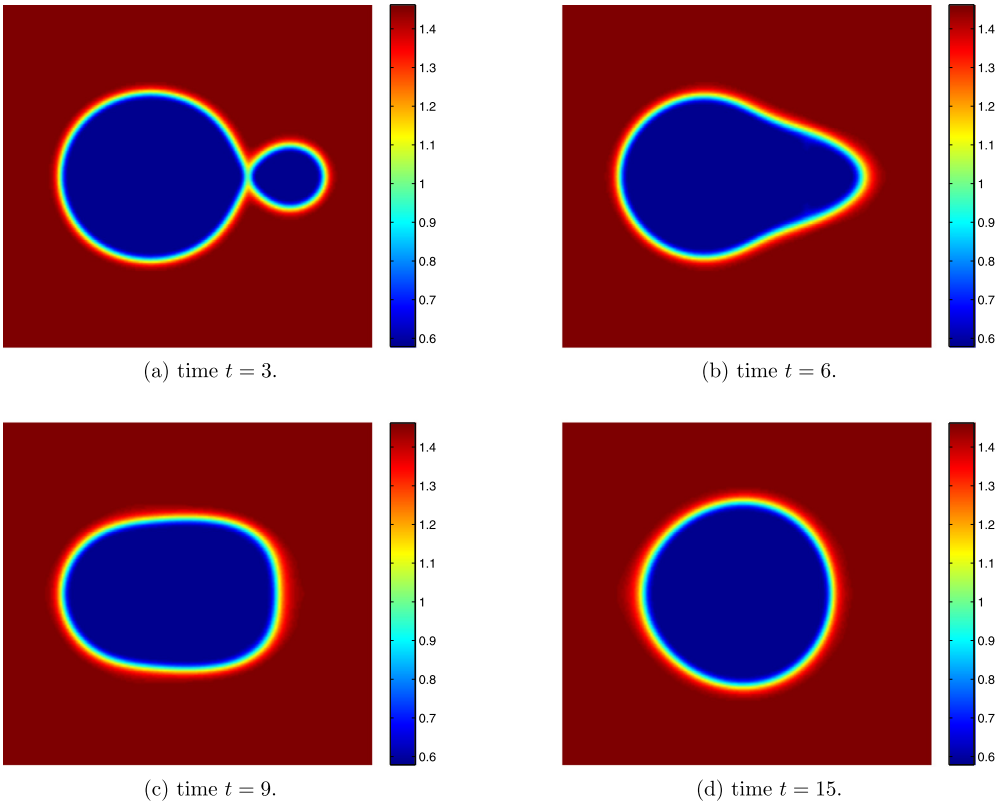

(a) time $t = 3$. (b) time $t = 6$.

(c) time $t = 9$. (d) time $t = 15$.

Fig. 25. Density ρ for two coalescing bubbles computed with the LDG discretization of the non-isothermal NSK equations using piecewise linear polynomials on a mesh with 200^2 square elements. The physical parameters are chosen as $\mathbb{R}e = 950$, $\mathbb{W}e = 34\,455$, $\mathbb{P}r = 0.843$, $C_v = 5.375$, and the Van der Waals EOS is set as (8). The initial condition is set as (40) with $\rho_1 = 0.579$, $\rho_2 = 1.462$ and $\theta_0 = 0.95$.

Appendix A

In this appendix we briefly discuss the derivation of the dimensionless form of the NSK equations and the definition of the dimensionless variables.

A.1. Dimensionless form of the isothermal NSK equations

The isothermal NSK equations are given by [29,5,14]

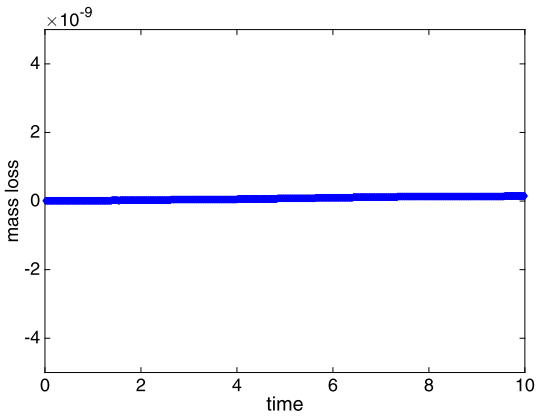

(a) mass loss

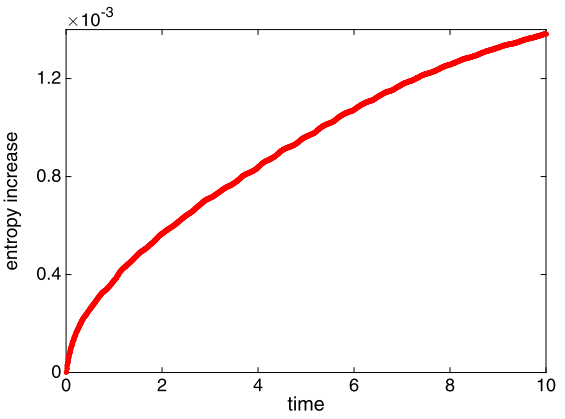

(b) entropy increase

Fig. 26. Evolution of mass loss and entropy on a mesh of 200^2 square elements as a function of time during the coalescence of two bubbles for the non-isothermal NSK equations, $\mathbb{R}e = 950$, $\mathbb{W}e = 34455$, $\mathbb{P}r = 0.843$, $C_v = 5.375$, and the Van der Waals EOS is set as (8). The initial condition is set as (40) with $\theta_0 = 0.989$, $\rho_1 = 0.6$, $\rho_2 = 1.4$.

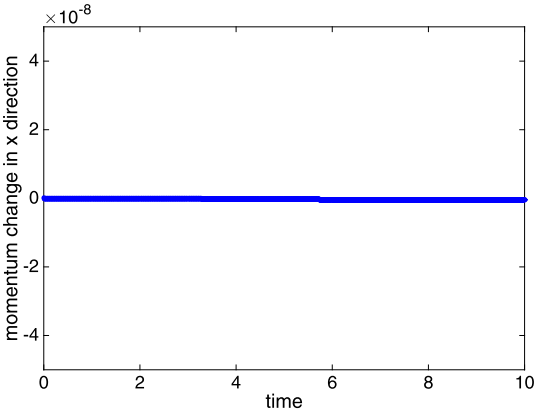

(a) momentum loss in x direction

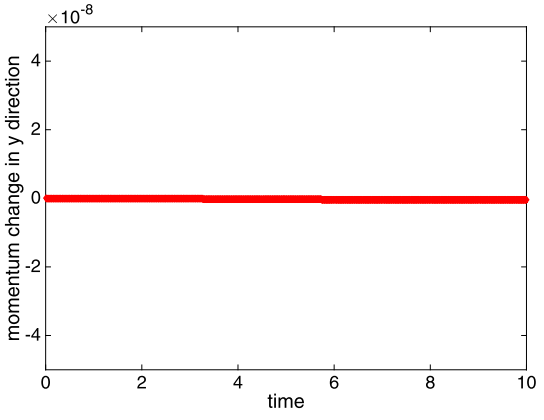

(b) momentum loss in y direction

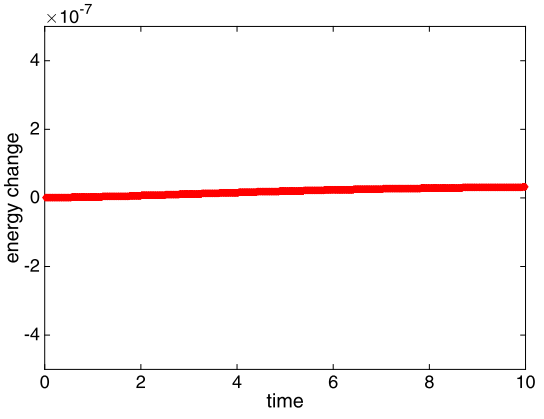

(c) energy loss

Fig. 27. Evolution of momentum in x and y direction on a mesh of 200^2 square elements as a function of time during the coalescence of two bubbles for the non-isothermal NSK equations, $\mathbb{R}e = 950$, $\mathbb{W}e = 34455$, $\mathbb{P}r = 0.843$, $C_v = 5.375$, and the Van der Waals EOS is set as (8). The initial condition is set as (40) with $\theta_0 = 0.989$, $\rho_1 = 0.6$, $\rho_2 = 1.4$.

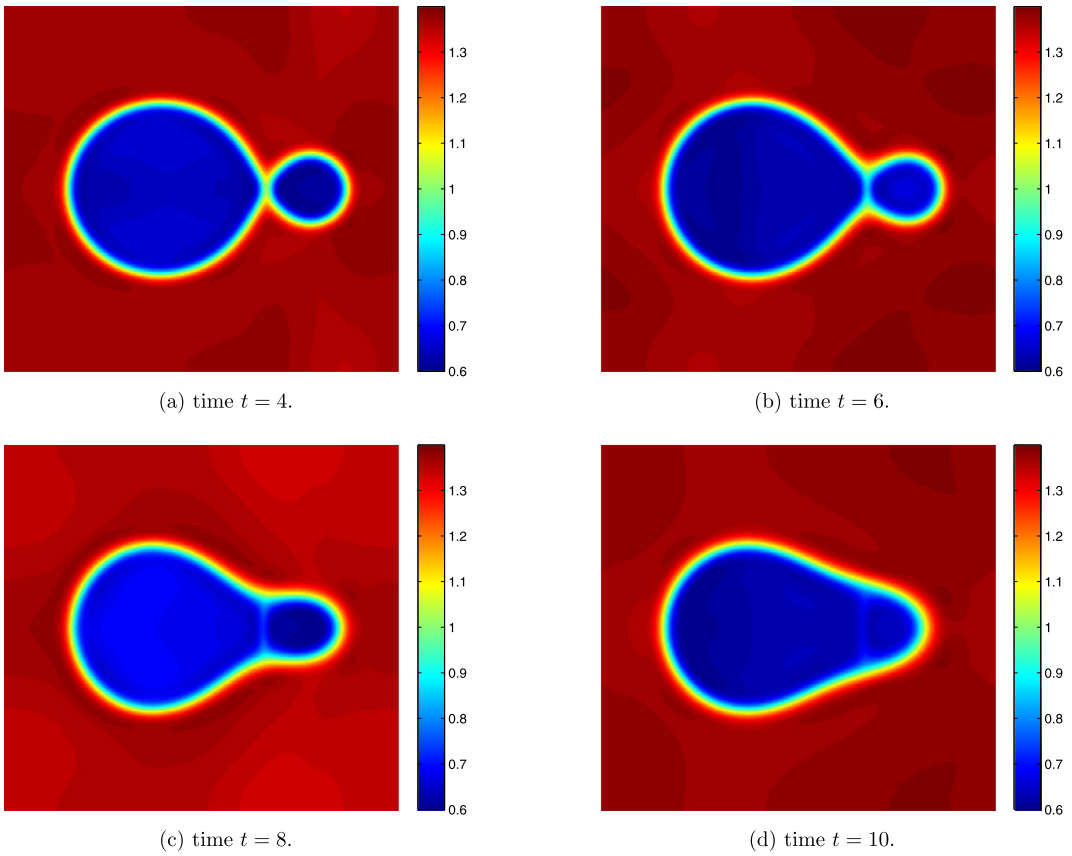

(a) time $t = 4$. (b) time $t = 6$.

(c) time $t = 8$. (d) time $t = 10$.

Fig. 28. Density ρ for two coalescing bubbles computed with the LDG discretization of the non-isothermal NSK equations using piecewise linear polynomials on a mesh with 200^2 square elements. The physical parameters are chosen as $\mathbb{R}e = 950$, $\mathbb{W}e = 34455$, $\mathbb{P}r = 0.843$, $C_v = 5.375$, and the Van der Waals EOS is set as (8). The initial condition is set as (40) with $\theta_0 = 0.989$, $\rho_1 = 0.6$, $\rho_2 = 1.4$.

$$\begin{aligned} &\frac{\partial \rho}{\partial t} + \nabla \cdot (\rho \mathbf{u}) = 0, \\ &\frac{\partial \rho \mathbf{u}}{\partial t} + \nabla \cdot (\rho \mathbf{u} \otimes \mathbf{u} + p\mathbf{I}) - \nabla \cdot \boldsymbol{\tau} - \nabla \cdot \boldsymbol{\xi} = \mathbf{0}, \end{aligned} \tag{41}$$

where ρ is the mass density, $\mathbf{u}$ the velocity. The viscous stress tensor $\boldsymbol{\tau}$ and the Korteweg stress tensor are defined as

$$\begin{aligned} \boldsymbol{\tau} &= \mu \left(\nabla \mathbf{u} + \nabla^T \mathbf{u} - \frac{2}{3} \nabla \cdot \mathbf{u} \mathbf{I} \right), \\ \boldsymbol{\xi} &= \lambda \left(\left(\rho \triangle \rho + \frac{1}{2} |\nabla \rho|^2 \right) \mathbf{I} - \nabla \rho \nabla^T \rho \right), \end{aligned} \tag{42}$$

with μ the viscosity coefficient and λ the capillary coefficient. The thermodynamic pressure is defined as

$$p = Rb \frac{\rho \theta}{b - \rho} - a\rho^2, \tag{43}$$

with θ the temperature, R the universal gas constant, a, b positive constants depending on the fluid.

The equations are made dimensionless using the following reference variables for the mass density, temperature and pressure

$$\rho_c = b, \ \theta_c = \frac{8ab}{27R}, \ p_c = ab^2.$$

The reference variable for the velocity is the average sound speed in the system $u_c = \sqrt{p_c / \rho_c}$ and the reference variable for time is $\frac{L}{u_c}$, with L the reference length. The Reynolds and Weber numbers are then defined as

$$\mathbb{R}e = \rho_c u_c L / \mu, \quad \mathbb{W}e = u_c^2 L^2 / (\rho_c \lambda).$$

Letting

$$\rho = \rho_c \widetilde{\rho},\ \mathbf{u} = u_c \widetilde{\mathbf{u}},\ p = p_c \widetilde{p},\ \theta = \theta_c \widetilde{\theta},$$

the governing equations (41) and (43) then can be transformed into their dimensionless form, resulting in (1)–(3).

A.2. Dimensionless form of the non-isothermal NSK equations

The non-isothermal NSK equations are given by [13,32]

$$\begin{aligned}
&\frac{\partial \rho}{\partial t} + \nabla \cdot (\rho \mathbf{u}) = 0,\\
&\frac{\partial \rho \mathbf{u}}{\partial t} + \nabla \cdot (\rho \mathbf{u} \otimes \mathbf{u} + p\mathbf{I}) - \nabla \cdot \tau - \nabla \cdot \boldsymbol{\xi} = \mathbf{0},\\
&\frac{\partial (\rho E)}{\partial t} + \nabla \cdot ((\rho E + p)\mathbf{u}) - \nabla \cdot ((\boldsymbol{\tau} + \boldsymbol{\xi}) \cdot \mathbf{u}) + \nabla \cdot \mathbf{q} + \nabla \cdot \mathbf{j}_E = 0,
\end{aligned} \tag{44}$$

with the definition of viscous stress tensor $\boldsymbol{\tau}$ and the Korteweg stress tensor defined in (42). The total energy density is given by

$$\rho E = \rho e + \frac{1}{2}\rho |\mathbf{u}|^2 + \frac{1}{2}\lambda |\nabla \rho|^2, \tag{45}$$

with the specific internal energy e defined as

$$e = C_v \theta - \frac{a}{M^2}\rho.$$

The Van der Waals equation of state for the non-isothermal NSK equations (44) is given by

$$p = \frac{R\theta\rho}{M - b\rho} - \frac{a}{M^2}\rho^2, \tag{46}$$

where C_v is the specific heat at constant volume, R the perfect gas constant, M the molar mass of the fluid, b the molar volume and a a constant modeling the interactions between the fluid particles. The heat flux $\mathbf{q}$ and energy flux $\mathbf{j}_E$ through the interface in (44) are defined as

$$\mathbf{q} = -K\nabla\theta, \quad \mathbf{j}_E = \lambda(\rho \nabla \cdot \mathbf{u})\nabla\rho, \tag{47}$$

with K the thermal conductivity.

Note that the form of the equation of state (46) for the non-isothermal NSK equations is different from (43) for the isothermal NSK equations, though they have a similar shape.

The reference variables for the mass density, temperature and pressure are, respectively,

$$\rho_c = M/(3b),\ \theta_c = \frac{8a}{27Rb},\ p_c = a/(27b^2).$$

The reference variable for the velocity is defined as $u_c = \sqrt{p_c/\rho_c}$ and the reference variable for time is $\frac{L}{u_c}$, with L the reference length. The Reynolds and Weber numbers are then equal to

$$\mathbb{R}e = \rho_c u_c L/\mu, \quad \mathbb{W}e = u_c^2 L^2/(\rho_c \lambda).$$

The Prandtl number and the reduced heat capacity are defined as $\mathbb{P}r = \mu C_v/K$, $\widetilde{C_v} = MC_v/R$.

The governing equations (44)–(47) then can be transformed into their dimensionless form, resulting in (6)–(9).

References

[1] R. Abeyaratne, J.K. Knowles, Implications of viscosity and strain-gradient effects for the kinetics of propagating phase boundaries in solids, SIAM J. Appl. Math. 51 (1991) 1205–1221.
[2] R. Alexander, Diagonally implicit Runge–Kutta methods for stiff ODE's, SIAM J. Numer. Anal. 14 (1977) 1006–1021.
[3] D.M. Anderson, G.B. McFadden, A.A. Wheeler, Diffuse-interface methods in fluid mechanics, Annu. Rev. Fluid Mech. 30 (1998) 139–165.
[4] G.K. Batchelor, An Introduction to Fluid Dynamics, Cambridge University Press, 1967.
[5] M. Braack, A. Prohl, Stable discretization of a diffuse interface model for liquid–vapor flows with surface tension, Modél. Math. Anal. Numér. 47 (2013) 401–420.
[6] D. Bresch, B. Desjardins, C.K. Lin, On some compressible fluid models: Korteweg, lubrication, and shallow water systems, Commun. Partial Differ. Equ. 28 (2003) 843–868.
[7] J.W. Cahn, J.E. Hilliard, Free energy of a nonuniform system. I. Interfacial free energy, J. Chem. Phys. 28 (1958) 258–267.
[8] J.R. Cash, Diagonally implicit Runge–Kutta formulae with error estimates, IMA J. Appl. Math. 24 (1979) 293–301.
[9] B. Cockburn, C.W. Shu, The local discontinuous Galerkin method for time-dependent convection–diffusion systems, SIAM J. Numer. Anal. 141 (1998) 2440–2463.

[10] F. Coquel, D. Diehl, C. Merkle, C. Rohde, Sharp and diffuse interface methods for phase transition problems in liquid–vapor flows, in: Numerical Methods for Hyperbolic and Kinetic Problems, vol. 7, 2005, pp. 239–270.
[11] J. Crank, Free and Moving Boundary Problems, Oxford University Press, 1997.
[12] R. Danchin, B. Desjardins, Existence of solutions for compressible fluid models of Korteweg type, Ann. Inst. Henri Poincaré, Anal. Non Linéaire 18 (2001) 97–133.
[13] J.L. Desmarais, J.G.M. Kuerten, Open boundary conditions for the diffuse interface model in 1-D, J. Comput. Phys. 263 (2014) 393–418.
[14] D. Diehl, Higher order schemes for simulation of compressible liquid–vapor flows with phase change, PhD thesis, Universität Freiburg, 2007.
[15] S.C. Eisenstat, H.F. Walker, Globally convergent inexact Newton methods, SIAM J. Optim. 4 (1994) 393–422.
[16] J. Giesselmann, C. Makridakis, T. Pryer, Energy consistent discontinuous Galerkin methods for the Navier–Stokes–Korteweg system, Math. Comput. 83 (2014) 2071–2099.
[17] H. Gomez, T.J. Hughes, X. Nogueira, V.M. Calo, Isogeometric analysis of the isothermal Navier–Stokes–Korteweg equations, Comput. Methods Appl. Mech. Eng. 199 (2010) 1828–1840.
[18] J. Haink, C. Rohde, Local discontinuous Galerkin schemes for model problems in phase transition theory, Commun. Comput. Phys. 4 (2008) 860–893.
[19] E. Hairer, G. Wanner, Solving Ordinary Differential Equation II. Stiff and Differential-Algebraic Problems, Springer, 2002.
[20] B. Haspot, Existence of global weak solution for compressible fluid models of Korteweg type, J. Math. Fluid Mech. 13 (2011) 223–249.
[21] H. Hattori, D. Li, Solutions for two-dimensional system for materials of Korteweg type, SIAM J. Math. Anal. 25 (1994) 85–98.
[22] H. Hattori, D. Li, The existence of global solutions to a fluid dynamic model for materials for Korteweg type, J. Partial Differ. Equ. 9 (1996) 323–342.
[23] C.W. Hirt, B.D. Nichols, Volume of fluid (VOF) method for the dynamics of free boundaries, J. Comput. Phys. 39 (1981) 201–225.
[24] D. Jamet, D. Torres, J.U. Brackbill, On the theory and computation of surface tension: the elimination of parasitic currents through energy conservation in the second-gradient method, J. Comput. Phys. 182 (2002) 262–276.
[25] C.T. Kelley, Iterative Methods for Linear and Nonlinear Equations, Society for Industrial and Applied Mathematics, 1995.
[26] M. Kotschote, Strong solutions for a compressible fluid model of Korteweg type, Ann. Inst. Henri Poincaré, Anal. Non Linéaire 25 (2008) 679–696.
[27] M. Kotschote, Strong solutions to the compressible non-isothermal Navier–Stokes equations, Adv. Math. Sci. Appl. 22 (2012) 319–347.
[28] M. Kotschote, Dynamical stability of non-constant equilibria for the compressible Navier–Stokes equations in Eulerian coordinates, Commun. Math. Phys. 328 (2014) 809–847.
[29] J. Liu, H. Gomez, J.A. Evans, T.J. Hughes, C.M. Landis, Functional entropy variables: a new methodology for deriving thermodynamically consistent algorithms for complex fluids, with particular reference to the isothermal Navier–Stokes–Korteweg equations, J. Comput. Phys. 248 (2013) 47–86.
[30] R.P. Pawlowski, J.N. Shadid, J.P. Simonis, H.F. Walker, Globalization techniques for Newton–Krylov methods and applications to the fully coupled solution of the Navier–Stokes equations, SIAM Rev. 48 (2006) 700–721.
[31] A. Pecenko, J.G.M. Kuerten, C.W.M. van der Geld, A diffuse-interface approach to two-phase isothermal flow of a Van der Waals fluid near the critical point, Int. J. Multiph. Flow 36 (2010) 558–569.
[32] A. Pecenko, L.G.M. Van Deurzen, J.G.M. Kuerten, C.W.M. van der Geld, Non-isothermal two-phase flow with a diffuse-interface model, Int. J. Multiph. Flow 37 (2011) 149–165.
[33] C. Rohde, On local and non-local Navier–Stokes–Korteweg systems for liquid–vapor phase transitions, Z. Angew. Math. Mech. 85 (2005) 839–857.
[34] L.M. Skvortsov, Diagonally implicit Runge–Kutta methods for stiff problems, Comput. Math. Math. Phys. 46 (2006) 2110–2123.
[35] L. Tian, Y. Xu, J.G.M. Kuerten, J.J.W. Van der Vegt, A local discontinuous Galerkin method for the propagation of phase transition in solids and fluids, J. Sci. Comput. 59 (2014) 688–720.
[36] G. Tryggvason, B. Bernard, E. Asghar, J. Damir, N. Al-Rawahi, W. Tauber, J. Han, S. Nas, Y.-J. Jan, A front-tracking method for the computations of multiphase flow, J. Comput. Phys. 169 (2001) 708–759.
[37] Y. Xu, C.W. Shu, A local discontinuous Galerkin method for the Camassa–Holm equation, SIAM J. Numer. Anal. 46 (2008) 1998–2021.
[38] Y. Xu, C.W. Shu, Local discontinuous Galerkin methods for high-order time-dependent partial differential equations, Commun. Comput. Phys. 7 (2010) 1–46.
[39] J. Yan, C.W. Shu, A local discontinuous Galerkin method for KdV type equations, SIAM J. Numer. Anal. 40 (2002) 769–791.
[40] P. Yue, J.J. Feng, C. Liu, J. Shen, A diffuse-interface method for simulating two-phase flows of complex fluids, J. Fluid Mech. 515 (2004) 293–317.